stage in which deflections at midspan differ from zero. This load condition represented in the middle scheme of Figure 3.2.

The third loading stage only takes place if $q > q_t$ and it represents the behavior when the structure is loaded with the portion of the live load for which the actuator works ($q_a = q - q_t$). The actuator elongates a magnitude enough to avoid any additional deflections at midspan from those obtained at stage 2. If stage 3 is studied independently, deflections at midspan are zero, replicating the behavior of a continuous beam, as depicted in the right scheme of Figure 3.2.

Figure 3.3 illustrates the deformed shape of the structure (scaled 200 times) when loaded progressively from 0 to 5 kN/m^2. The aim of this figure is to show the evolution of the deflections at the deck when using the partially smart system. In this case, the live load threshold has been set to 2 kN/m^2. When the live load is lower than q_t the actuator does not work, and the shape acquired by the deck depends on the relative stiffness between the deck and the cable-stayed system. Once q overpasses q_t, the actuator starts working and additional deflections at midspan are inhibited. The position of the maximum displacement will progressively move from midspan to the supports.

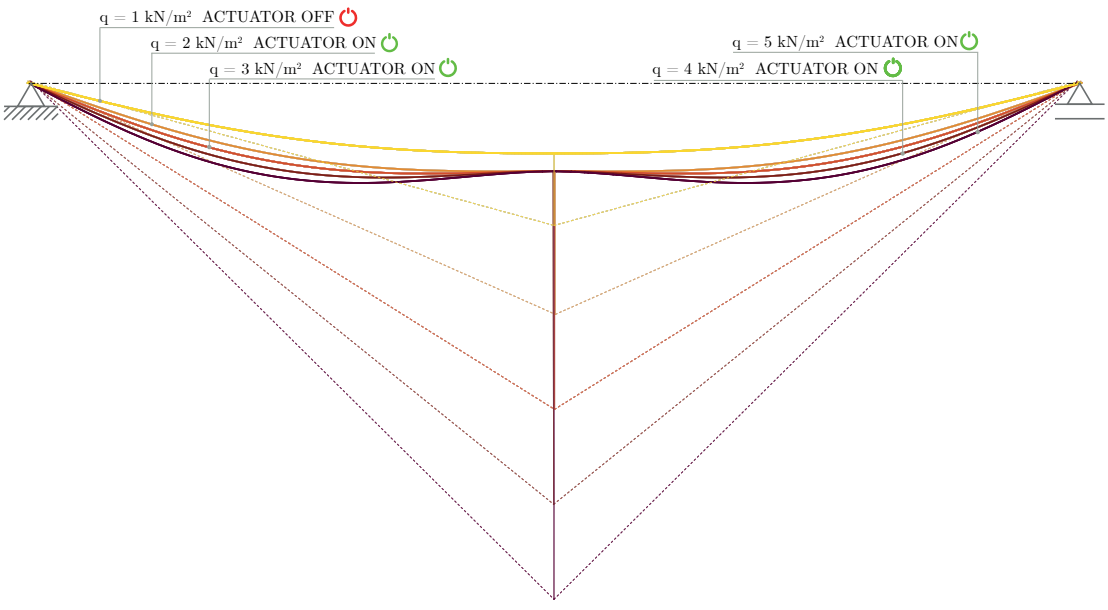

Figure 3.3: Deformed shape of the deck under increasing live loads. Example for a live load threshold of $q_t = 2$ kN/m^2. (Deformation scaled 200 times).

A partially smart strategy allows a more efficient distribution of bending moments along the deck. When considering the sum of the three loading stages, it is possible to

obtain very similar absolute values for the maximum positive and negative bending moments. Additionally, the overall deflection is effectively reduced not only at midspan but along the entire deck. However, in contrast to these benefits achieved on the deck, the load carried by the cable-stayed system increases. Therefore, an increased cross-sectional area will be required.

Regarding the unloading stage of the structure, two different approaches are proposed, represented in Figure 3.4. In the top row, two identical graphs are plotted, showing the loading sequence. In the second row, the displacements at midspan versus the time are displayed. The last row shows the actuator stroke (elongation) for each loading strategy.

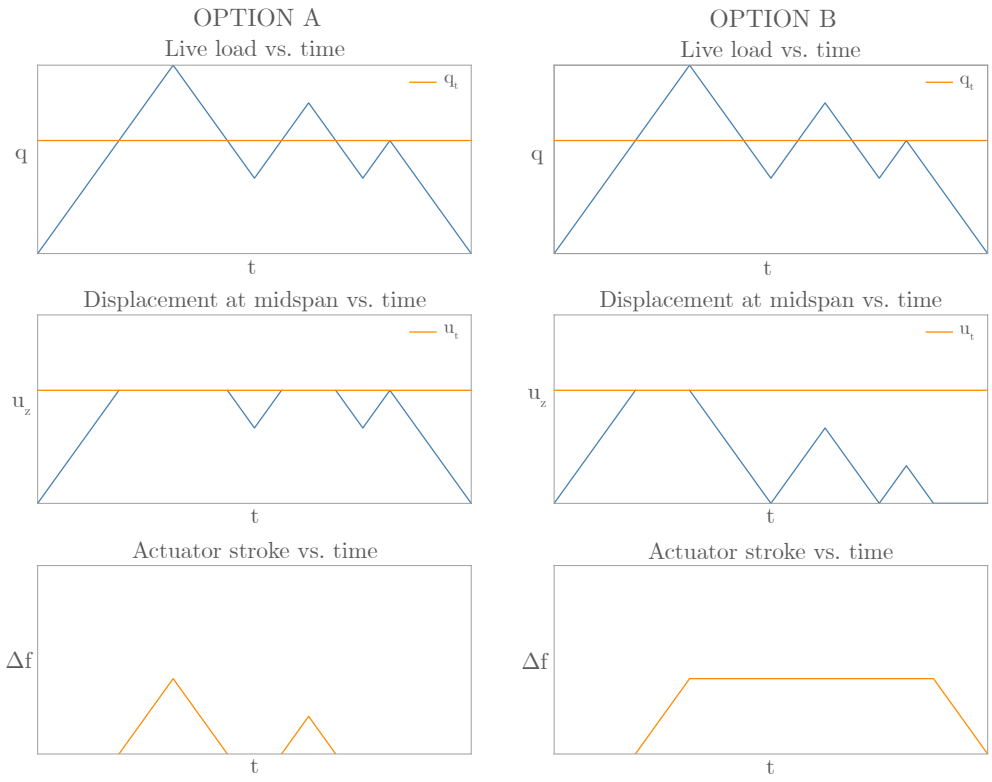

Figure 3.4: Unloading strategies.

In the first option (A), the unloading is identical to the loading: when the vertical deflection at midspan lowers from the maximum permissible value, the actuator progressively contracts until it reaches its original position. On the other hand, the second unloading strategy (B), establishes a lower limit for the deflection, from which the actuator starts to contract. In the example plotted in Figure 3.4, the lower limit is set to $u_z = 0$. Thus, for deflections between 0 and u_z, the actuator does not move. Following this strategy, the movements of the actuator are minimized, thereby reducing the energy consumption. This

is possible because the actuator only consumes energy while moving, (i.e. if it is locked in its position, it does not consume any energy). Another advantage of this strategy is that it works as a filter of the displacement signal, preventing the actuator to uselessly move around the threshold.

Considering the above, option B is considered the optimal strategy to be used during the unloading stage. Although this is not implemented in the theoretical study of the structural behavior described in this part, it will be considered for the experimental prototype discussed in Chapter 7.

3.3 Design methodology

3.3.1 Geometry and materials

The reference footbridge, as represented in Figure 3.5, has a span length (L) equal to 50 meters and a rise of the bridge (f) of 5 meters, resulting in a span-to-rise ratio (L/f) equal to 10, which is a common value in under-deck cable-stayed systems [4]. The load-bearing element of the deck is a longitudinal steel beam, which has a cross-section based on a 25-mm-thick square hollow shape and a fixed width (b) of 0.8 meters. A total deck width (B) of 4 meters is considered.

The height of the deck (h) and the area of the cable-stayed system (A') are the variables to be defined in the design. When using the FE methodology (Chapter 5), only discrete values are assigned to h and A', which correspond to manufacturer specifications, whereas in the analytical formulation (Chapter 4), those values are obtained mathematically and can be any within a continuous range.

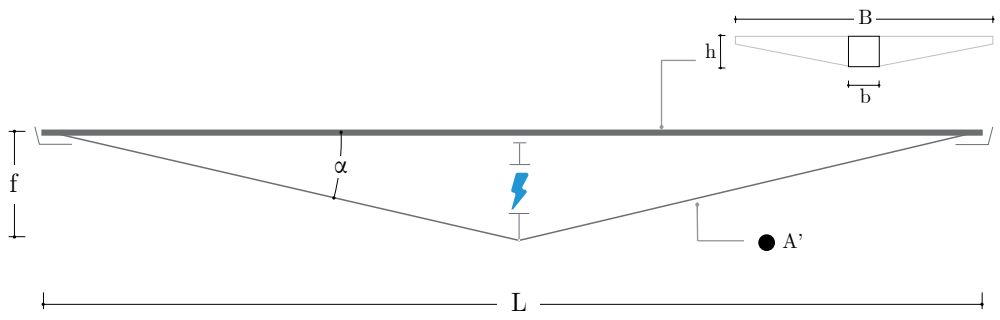

Figure 3.5: Dimensions of the reference smart under-deck cable-stayed footbridge.

The beam is made of steel S235 ($f_{sy} = 235$ MPa and $E_s = 210$ GPa). Fully locked cables are used in the cable-stayed system. The mechanical characteristics of these elements depend on the cross-sectional area and the manufacturer. As a simplification, as recommended by Part 1–11 of Eurocode 3 [22], the nominal cross-sectional area (A') is taken as the multiplication of the surface area (A'_s) per the fill-factor ($f = 0.88$, as proposed by the same code for fully locked cables). In addition, the same code indicates the mechanical properties: $f_{uk} = 1570$ MPa and $E'_s = 160$ GPa. Sag effects in the cable are neglected due to its short length.

3.3.2 Design criteria

The structure is designed according to the Eurocodes, applying the values established in the Spanish National Annexes when necessary. The applicable Eurocodes are:

- Eurocode 0: Basis of structural design [77].
- Eurocode 1: Actions on structures [78].
- Eurocode 3: Design of steel structures [22]. Specifically, the following parts are used:
  - Part 1–1: General rules and rules for buildings.
  - Part 1–11: Design of structures with tension components.

The dynamic verifications are done following the HiVoSS Guidelines [79].

The following steps define the rules for action combinations, specify the actions to be considered, and determine the applicable limit states for the deck and the cable-stayed system.

Definition of actions

The permanent loads considered in the structural analysis are the self-weight of the longitudinal beam and a superimposed dead load estimated as 4 kN/m^2. These loads are considered to be uniformly distributed along the deck. To simplify the analysis, the self-weight of the beam is assumed to be 1 kN/m^2 in the analytical formulation. However, in the numerical analysis, the actual self-weight is considered.

Regarding the variable loads, only the traffic load is taken into account. Wind and thermal actions are neglected, as they do not provide any significant information regarding the functioning of the smart system. The design live load (q_d), as established by Part 2 of Eurocode 1 [78] has a value of 5 kN/m^2 in footbridges. In Chapter 4, this load is uniformly

applied throughout the entire span. In Chapter 5, where the structure is calculated thought a Finite Element Model (FEM), the live load is applied in different positions to obtain the worst scenario in terms of deflections and bending moments. These positions are: i) all the deck is loaded, ii) only half span is loaded, and iii) only half section is loaded.

Additionally, in the FEM, the vertical live load is combined with the horizontal forces that are transferred to the bridge deck by the pedestrian parapets. According to the Spanish National Annex, this is considered as a distributed load of 1.5 kN/m^2 applied on the top of the parapet, located at 1.0 meters from the top of the deck. The horizontal longitudinal load acting on the surface of the deck is neglected.

General rules for combination of actions

The verification of the Ultimate Limit State (ULS) is carried out according to Eurocode 0 [77], which requires satisfying $E_d \leq R_d$, where E_d is the design value of the effects of the actions and R_d is the design value of the corresponding resistance. The former is calculated from the combination of actions according to the next equation:

$$\sum_{j \leq 1} \gamma_{G,j} G_{k,j} + \gamma_P P + \gamma_{Q,1} Q_{k,1} \tag{3.1}$$

Where $G_{k,j}$ are the characteristic values of the permanent loads, P is the representative value of the force in the cable-stayed system and $Q_{k,1}$ is the traffic action, which is the only variable action considered in this work.

Each action is multiplied by the corresponding partial factor which, according to the Spanish national Annex 1 of the EN 1990 [77], have the following values:

- $\gamma_{G,j}$ is equal to 1.35 for unfavorable effects and 1.00 for favorable effects.
- γ_P is equal to 1.35 for unfavorable effects and 1.00 for favorable effects.
- $\gamma_{Q,i}$ is equal to 1.35 for unfavorable traffic loads and 0.00 if favorable.

As indicated in Section 2.2.2, the permanent loads and the prestressing force are considered as independent actions, each multiplying its corresponding (favorable or unfavorable) partial factor.

The verification of the characteristic Serviceability Limit State (SLS) is carried out with the following combination of actions, according to Eurocode 0 [77]:

$$\sum_{j \leq 1} G_{k,j} + P + Q_{k,1} \tag{3.2}$$

Finally, for the accidental combination of actions, the following equation will apply:

$$\sum_{j\leq 1} G_{k,j} + P + A_d + \psi_{1,1} Q_{k,1} \tag{3.3}$$

In the previous equation, A_d is the design value of the accidental action, which will be equal to 0 to refer to a situation following an accidental event. A_d is combined with the frequent value of the main variable load, obtained as the multiplication of its characteristic value times the factor psi_1, equal to 0.4 for the pedestrian traffic load.

Definition of the applicable limit states

The applicable limit states in each part of the structure (i.e., the steel beam and the cable-stayed system), are defined next.

As indicated in Section 2.2.2, the cable-stayed system is designed according to Part 1–11 of Eurocode 3 [22], employing fully locked cables (group B tension components). The following limit states are considered:

$$\mathrm{F_{ULS}} \leq \frac{F_{uk}}{1.5} \tag{3.4}$$

$$\mathrm{F_{SLS}} \leq 0.45 \cdot F_{uk} \tag{3.5}$$

Where $\mathrm{F_{ULS}}$ and $\mathrm{F_{SLS}}$ are, respectively, the design values of the axial forces at ULS and SLS. The characteristic value of the breaking strength (F_{uk}) is defined as $F_{uk} = A'\ f_{uk}$, being f_{uk} the Guaranteed Ultimate Tensile Strength (GUTS), taken as 1570 MPa, and A' the cross-sectional area of the cable-stayed system. Equations 3.4 and 3.5 do not considered any measures to minimize bending stresses at the anchorages. Additionally, fatigue in the cable-stayed system is verified, as it will be detailed in Section 5.4.2.

ULS and SLS are also the applicable limit states considered in the deck, according to Part 1–1 of Eurocode 3 [22]. As a simplification, no plastic behavior is considered. The ULS verification according to Eurocode 3 [22] is:

$$\sigma_{Ed} \leq \frac{f_{sy}}{\gamma_{M0}} \tag{3.6}$$

Where σ_{Ed} is the design value of the maximum stress on the deck at ULS, which is limited by the yield strength of the structural steel (f_{sy}). The partial factor for the material (γ_{M0}) is taken as 1.0, as recommended in Section 6.1 of Part 1–1 of the Eurocode 3 [22]. Additionally, buckling in the deck will be checked.

With respect to SLS, a simplified conservative approach is followed by adopting the limitation outlined in the Spanish Annex of Eurocode 0 [77] for footbridges. In this approach, the maximum displacement on the deck ($u_{z,\max}$) caused by the frequent live load ($\psi_1\ q_d$) is limited to $L/1200$, being L the span of the footbridge. According to the same standard, by fulfilling this limitation, the vibration limit state is implicitly satisfied, so there is no requirement for a separate verification. However, due to the singularity of the smart structure, a dynamic analysis is performed in Section 5.4.1.

When applying this limitation ($u_{z,\max} \leq L/1200$), the sequence in which the live load is resisted must be considered, as illustrated in Figure 3.1. When q_t exceeds the frequent live load (i.e., $q_t > 0.40\ q_d$), the maximum displacement is checked before the actuator has begun to operate. Consequently, the structural verification for SLS in the deck is identical for values of q_t/q_d between 0.4 and 1.

Additionally, the possible scenario of an interruption of the power supply must be considered. The linear actuators are instantly self-locked if there is a power shortage, so the structure would start to work as a conventional under-deck cable-stayed structure. This will be treated as an Accidental Limit State (ALS) for which, according to Equation 3.3, the structure should be able to resist the permanent loads plus the frequent live load. In Chapter 5, the FEM will be used to verify that both the deck and the cable-stayed system are able to resist this scenario.

The ALS of the cable breakage has been excluded from this study due to the conceptual nature of the work. The ability of the structure to withstand this scenario can be accomplished by incorporating adequate redundancy into the cable-stayed system. An effective approach is to employ multiple cables (maintaining the required total cross-sectional area), as illustrated in the examples of under-deck cable-stayed bridges showcased in Section 2.2.

4

Analytical formulation

4.1 Theoretical framework and methodology

This chapter focuses on the analytical study of the structural behavior of the single-span smart under-deck cable-stayed footbridge illustrated in Figure 3.5. This study is done by dividing the load scenarios into three stages, as described in Section 3.2.2. The different load conditions are represented in Figure 4.1.

For the first and third loading stages, the structure is equivalent to a two-span continuous beam in which the actuator behaves as a fixed support. This allows for an independent study of the deck and the under-deck cable-stayed system. However, for the second loading stage, the combined behavior of the system needs to be considered. To address this, the formulation defined by Ruiz-Terán [4], [15], [80], as introduced in Section 2.2, is used. This formulation allows to successfully study the behavior of structures with under-deck cable-stayed systems.

Next, the formulation used in each load condition is derived, explaining the corresponding hypothesis.

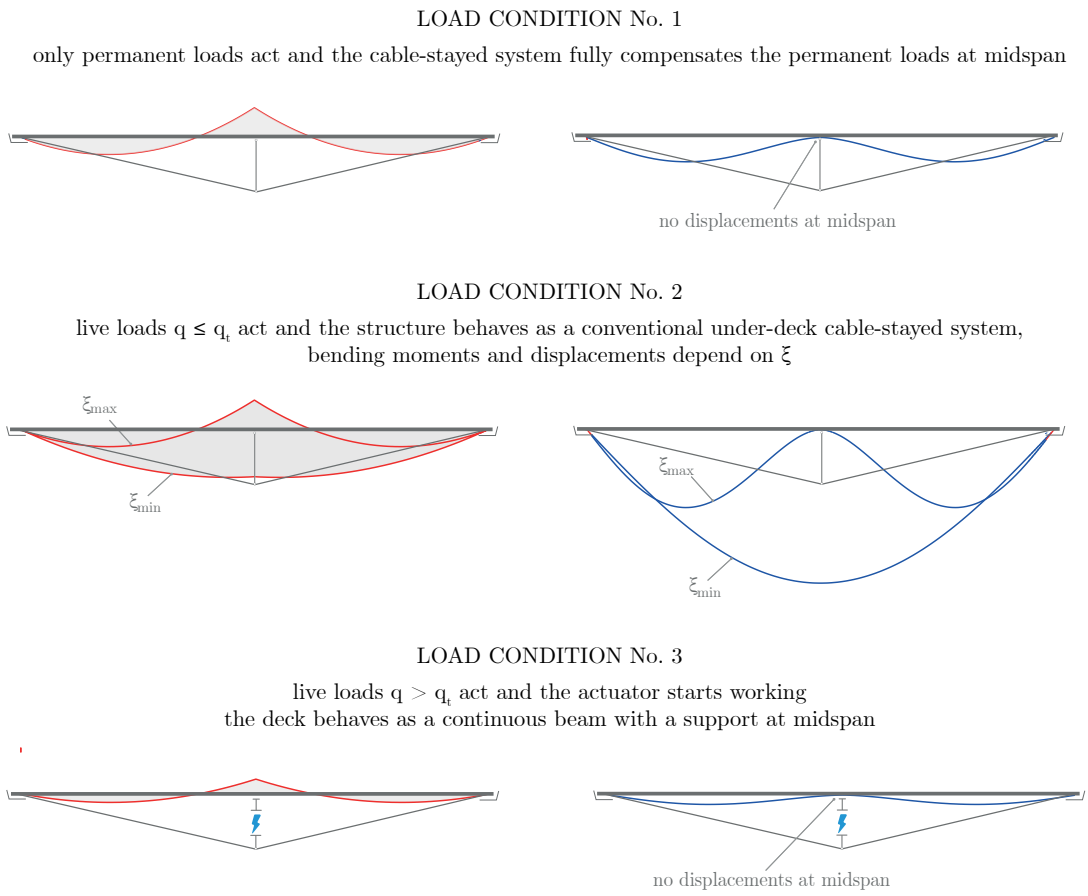

Figure 4.1: Bending moments (left, in red) and displacements (right, in blue), in the deck for the different load conditions.

Load condition No. 1. Permanent state

The permanent state is composed by the self-weight of the deck (g_1), the superimposed dead load ($g_2 = 4$ kN/m^2) and the initial prestress force given to the stays. In this chapter, as a simplification, the self-weight of the deck is assumed as 1 kN/m^2 acting in the total width of the deck (B), equal to 4 m. Thus, the permanent load is $g = 20$ kN/m.

The structural behavior during the permanent state depends on the portion of the permanent loads compensated by the cable-stayed system (ρ) [4]. In all the cases presented in Part II, the system is designed to completely balance the permanent loads at midspan ($\rho = 100$ %), allowing to halve the calculation span for permanent loads and, as a consequence, to reduce by a fourth the bending moments in the beam if compared to an equivalent structure without any tensioning system. This means that the structural behavior of the beam is

equivalent to a continuous beam with two equal spans, with the strut acting as an intermediate fixed support (i.e., the deflection at midspan is zero). This behavior is represented in the top row of Figure 4.1.

To evaluate stresses in the deck and the cable-stayed system, the axial forces and bending moments are obtained. First, the vertical upward reaction (R_0) transferred by the strut to the under-deck cable-stayed system is calculated. The equation is equivalent to the middle support reaction of a continuous beam with two spans of length $L/2$:

$$R_0 = \rho \cdot \frac{5}{8} \cdot L \cdot g \tag{4.1}$$

By applying force equilibrium at the node where the cable-stayed and the strut meet, the axial force in the cable (F_0) and the compression force in the beam (H_0), which depend on the angle formed between the under-deck cable-stayed system and the deck (α), can be determined. The configuration of the strut, which is perpendicular to the beam and articulated at both ends, ensures that the compression force remains constant along the beam.

$$F_0 = \frac{R_0}{2 \cdot sin\alpha} \tag{4.2}$$

$$H_0 = \frac{R_0}{2 \cdot tan\alpha} = \text{constant} \tag{4.3}$$

The bending moments in the beam are evaluated in two sections, coincident with the maximum negative ($x = L/2$) and positive ($x = 3L/16$) bending moments.

$$M_{0,x=\frac{L}{2}} = -\frac{L^2 \cdot g}{32} \tag{4.4}$$

$$M_{0,x=\frac{3L}{16}} = \frac{9 \cdot L^2 \cdot g}{512} \tag{4.5}$$

Load condition No. 2. Live load $\mathbf{q < q_t}$

The second loading stage corresponds to the conventional under-deck cable-stayed system, which carries, at maximum, the live load threshold (q_t). As explained by Ruiz-Terán [4] and represented in the second row of Figure 4.1, the load distribution between the beam and the cable-stayed system is determined by the efficiency of the cable-stayed system (ξ). While the parameter ξ represents the distribution of the live load between the deck and the cable-stayed system, it does not have any influence in the permanent state. In the same way, ρ does not have any effect on the live load distribution.

In this load condition, the structural behavior of the deck can be resembled to a simply supported beam with a spring support at midspan, whose stiffness depends on ξ. Figure 4.1 shows that the bending moment distribution strongly depends on ξ and, consequently, for most values of ξ deflections are not zero at midspan. The higher the value of ξ, the closer the behavior of the deck to that of a continuous beam (see ξ_{max} in Figure 4.1). On the other hand, the lower the value of ξ, the lower is the efficiency of the cable-stayed system, with the beam bending moment distribution converging to that of a simply supported beam (see ξ_{min} in Figure 4.1).

Next, the derivation of ξ proposed by Ruiz-Terán [4] is presented. Although the equation only depends on the relative stiffness of the deck with respect to the cable-stayed system (χ), its formulation would change for different support conditions and types of loads. For a simply-supported beam loaded with a uniformly distributed load, ξ is obtained as follows:

$$\xi = \frac{5}{4} \cdot \frac{1}{1 + 12\chi} \tag{4.6}$$

The parameter χ is defined as:

$$\chi = \chi_I + \frac{\chi_I}{\chi_A} \tag{4.7}$$

Where χ_I is the adimensional parameter that determines the structural behavior of the system if axial deformation in the deck is not considered:

$$\chi_I = \frac{E_s \cdot I}{4 \cdot f^2 \cdot \cos^3 \alpha \cdot E'_s \cdot A'} \tag{4.8}$$

And χ_A is the adimensional parameter that considers the axial deformation in the deck:

$$\chi_A = \frac{E_s \cdot A}{\cos^3 \alpha \cdot E'_s \cdot A'} \tag{4.9}$$

Where E_s, I and A are, respectively, the Young Modulus, the inertia and the area of the deck and E'_s and A' are, respectively, the Young Modulus and the cross section (nominal area) of the cable-stayed system.

If instead of a uniformly distributed load, a point load (Q) at the strut location is considered, the formulation of ξ would be as follows:

$$\xi_Q = \frac{1}{1 + 12\chi} \tag{4.10}$$

The axial force in the midspan strut due to a concentrated load (R_Q) is the fraction of Q carried by the stays. It is obtained as a product of Q times the efficiency of the cable-stayed system (ξ_Q). The remaining part of Q is resisted by bending of the deck.

$$R_Q = Q \cdot \xi_Q = Q \cdot \frac{1}{1 + 12\chi} \tag{4.11}$$

An analogue equation can be obtained for the axial force in the midspan strut due to a uniformly distributed load (R_q), where $5/8 \cdot L \cdot q$ is the portion of q applied in the influence zone of the strut:

$$R_q = (\frac{5}{8} \cdot L \cdot q) \cdot \frac{1}{1 + 12\chi} \tag{4.12}$$

Which can also be expressed as:

$$R_q = \frac{5}{8} \cdot L \cdot q \cdot (\frac{4}{5} \cdot \xi) = \frac{1}{2} \cdot L \cdot q \cdot \xi \tag{4.13}$$

In the previous equation, ξ is multiplied by $4/5$ in order to not take into account the influence zone of the strut twice, as it is already considered in the equation of ξ.

The axial forces in the stays and the compression force in the deck are determined using a similar approach as in the permanent state analysis:

$$F_q = \frac{R_q}{2 \cdot sin\alpha} = \frac{q \cdot L}{4 \cdot sin\alpha} \cdot \xi \tag{4.14}$$

$$H_q = \frac{q \cdot L}{4 \cdot tan\alpha} \cdot \xi \tag{4.15}$$

As a simplification, the bending moments will be evaluated at the same sections as in the previous load condition ($x = L/2$ and $x = 3L/16$), although the location of the maximum positive bending moment will depend on ξ. When ξ is low, this simplification entails important differences with the results obtained thought the FEM (Chapter 5).

$$M_{q,x=\frac{L}{2}} = \frac{1}{8} \cdot q \cdot L^2 \cdot (1 - \xi) \tag{4.16}$$

$$M_{q,x=\frac{3L}{16}} = \frac{3}{64} \cdot q \cdot L^2 \cdot (\frac{13}{8} - \xi) \tag{4.17}$$

The bending moment distribution in the deck varies significantly depending on ξ. Figure 4.1 shows the behavior of the deck for the extreme values of ξ. While these extremes are theoretical, the structural behavior under these conditions would be as follows:

- Minimum efficiency of the cable-stayed system: $\xi = 0$. This value of ξ would imply that χ is infinite, representing a case in which the deck is infinitely stiffer than the cable-stayed system and, therefore, the latter does not withstand any live loads. The structure behaves as a simply supported beam.
- Minimum efficiency of the cable-stayed system. For a uniformly distributed load, ξ would reach a maximum value of $\xi_q = 5/4$, which implies that $\chi = 0$ (i.e., the stiffness of the cable-stayed system is infinitely higher than that of the deck and the strut behaves as a pin support). The deck would behave as a continuous beam.
  If the live load was a point load (Q), the maximum would be $\xi_Q = 1$ and there would not be any bending in the deck, as all the live load would descend directly through the strut to the stays, whose stiffness would be infinite compared to that of the deck. For a uniformly distributed load and a value of $\xi_q = 1$, there would be no bending at the midspan section.

Load condition No. 3. Live load $\mathbf{q > q_t}$

The third load condition begins when the live load exceeds q_t. The actuator resists the additional load ($q_a = q - q_t$) by extending until it reaches a length where deflections caused by q_a at midspan are zero, acting as a pin support. As a result, the load applied near the strut directly transfers to the cable-stayed system, so the deck behaves as a continuous beam for q_a, and the equations for the section forces are equivalent to those described for the permanent state. If considering the loading sequence, the total deflection at midspan in this loading stage is equal to the deflection due to load condition No. 2. The elongation of the actuator results in an increase in the rise (Δf), which leads to an increase in α. However, since the magnitude of this increase is small, it is neglected.

Table 4.1 compiles the section forces in the three load conditions, both in the deck and in the cable-stayed system. Bending is calculated at the midspan section ($x = L/2$) and in the section located at a distance of $x = 3L/16$ from the end support. These equations are combined according to Section 3.3.2 to obtain the design values of the section forces.

Table 4.1 Summary of the equations to evaluate axial forces in the strut and the cable-stayed system and bending moments in the deck, for the different load conditions.

	Permanent state (g)	**Live loads**		
		$q \leq q_t$	**$q > q_t$**	
		Conventional cable-stayed behavior only	**Conventional cable-stayed behavior (q_t)**	**Smart behavior ($q_a = q - q_t$)**
Axial force in the strut [kN]	$R_0 = \frac{5}{8} \cdot L \cdot g$	$R_q = \frac{1}{2} \cdot L \cdot q \cdot \xi$	$R_{q_t} = \frac{1}{2} \cdot L \cdot q_t \cdot \xi$	$R_{q_a} = \frac{5}{8} \cdot L \cdot q_a$
Axial force in the stays [kN]	$F_0 = \frac{5}{16} \cdot \frac{L \cdot g}{sin\alpha}$	$F_q = \frac{q \cdot L}{4 \cdot sin\alpha} \cdot \xi$	$F_{q_t} = \frac{q_t \cdot L}{4 \cdot sin\alpha} \cdot \xi$	$F_{q_a} = \frac{5}{16} \cdot \frac{q_a \cdot L}{sin\alpha}$
Bending in the deck at midspan [kNm]	$M_{0,\frac{L}{2}} = -\frac{L^2 \cdot g}{32}$	$M_{q,\frac{L}{2}} = \frac{1}{8} \cdot q \cdot L^2 \cdot (1 - \xi)$	$M_{q_t,\frac{L}{2}} = \frac{1}{8} \cdot q_t \cdot L^2 \cdot (1 - \xi)$	$M_{q_a,\frac{L}{2}} = -\frac{q_a \cdot L^2}{32}$
Bending in the deck at x=3L/16 [kNm]	$M_{0,\frac{3L}{16}} = \frac{9 \cdot L^2 \cdot g}{512}$	$M_{q,\frac{3L}{16}} = \frac{3}{64} \cdot q \cdot L^2 \cdot (\frac{13}{8} - \xi)$	$M_{q_t,\frac{3L}{16}} = \frac{3}{64} \cdot q_t \cdot L^2 \cdot (\frac{13}{8} - \xi)$	$M_{q_a,\frac{3L}{16}} = \frac{9 \cdot q_a \cdot L^2}{512}$

In the deck, the design bending moment (M_{Ed}) and the design compression force (H_{Ed}) are used to calculate the design stress (σ_{Ed}), which is obtained as the maximum normal stress between the values obtained at $x = L/2$ and $x = 3L/16$. Stresses due to shear forces are neglected.

$$\sigma_{Ed} = \frac{M_{Ed} \cdot y}{I} + \frac{H_{Ed}}{A} \tag{4.18}$$

To assess SLS in the beam, the maximum vertical displacement of the deck (u_z) is calculated assuming it is at $x = 3L/16$. It is estimated as a sum of two terms, as shown in Equation 4.19. The first term corresponds to the displacement at midspan due to the second load condition, which depends on ξ [4]. The second term represents the relative vertical displacement between the sections located at $x = 3L/16$ and at $x = L/2$. In a simplified way, this term is calculated considering the beam as continuous for both the second and third loading stages. With this assumption, the calculated deflection is always higher than the real one, thus the design is conservative.

$$u_{z(x=3L/16)} = \frac{5 \cdot (0.4 \cdot k_t \cdot q_t) \cdot L^4}{384 \cdot E \cdot I} \cdot (1 - \frac{4}{5} \cdot \xi) + \frac{(0.4 \cdot (k_t \cdot q_t + k_a \cdot q_a)) \cdot L^4}{2960 \cdot E \cdot I} \tag{4.19}$$

In order to take into account the loading sequence, each portion of the live load is multiplied by two factors:

- If $q_t/q_d \geq 0.4$: $k_t = 0.4/(q_t/q_d)$ and $k_a = 0$
- If $q_t/q_d < 0.4$: $k_t = 1$ and $k_a = (0.4 - q_t/q_d)/(1 - q_t/q_d)$

To conclude, the assumptions done in this methodology are summarized:

- The methodology assumes that all loads are uniformly distributed along the entire deck, disregarding the more restrictive scenario where the live load is applied only to half of the span. This assumption is addressed in the FE analysis.
- The maximum positive bending moment is always considered at $x = 3L/16$. However, this assumption is only true for fully smart systems ($q_t/q_d = 0.0$). The error will increase as q_t/q_d grows and ξ decreases, situations for which the position of the maximum positive bending moment will be closer to midspan.
- The maximum displacement is assumed to be located at $3L/16$ and calculated as the maximum displacement at midspan plus the displacement at $3L/16$, considering the strut acting as a fixed support. Again, this is not the case in partially smart systems. This simplification provides conservative results.

Despite these simplifications, the presented methodology provides a reasonable approximation to design smart under-deck cable-stayed structures. It offers useful preliminary results and serves as a convenient tool for conducting various parametric analyses. Nonetheless, it should be noted that the results obtained using this methodology cannot be directly compared to those obtained in Chapter 5, which are obtained through a more refined numerical analysis. However, they can be compared among themselves for relative evaluations.

4.2 Design workflow

The objective of this design procedure is to determine the minimum cross-sectional area of the stays (A') and the minimum height of the beam (h), while fulfilling ULS and SLS.

Since the design of h and A' is directly correlated (if the stiffness of one element is reduced, the other needs to be increased), a compromise has to be reached. The selected design criterion consists in defining h and A' to strictly fulfill the most restrictive limit state (i.e., the material utilization is equal to 1).

Figure 4.2 plots schematically the solutions (pairs of h and A') that strictly fulfill each limit state independently. This graph corresponds to one of the cases designed in Section 4.3, which depends on the value of q_t/q_d.

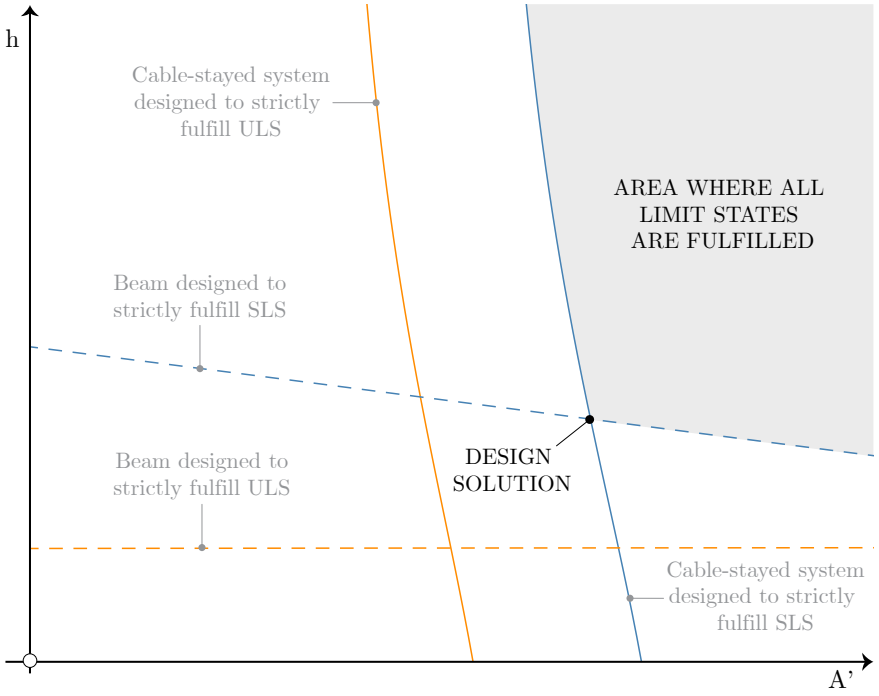

Figure 4.2: Solutions of h and A' fulfilling a specific limit state.

The multiple solutions that fulfill all limit states (gray area) are delimited by two curves, each one corresponding to the most restrictive limit state in each element. In this specific case, SLS criteria (blue curves) govern the design of both elements. The intersection of these two curves indicates the point where both limit states are fulfilled simultaneously. This is the pair of h and A' used in the design.

It is worth mentioning that the criterion to define the design solution can be varied to optimize specific targets (e.g. cost, weight, CO_2 emissions, etc.). This topic is briefly addressed in the future research section.

As mentioned, the load distribution between both elements depends on χ. Thus, the design of each element depends both on h and A'. In order to calculate the desired solution, an iteration process is followed (graphically shown in Figure 4.3).

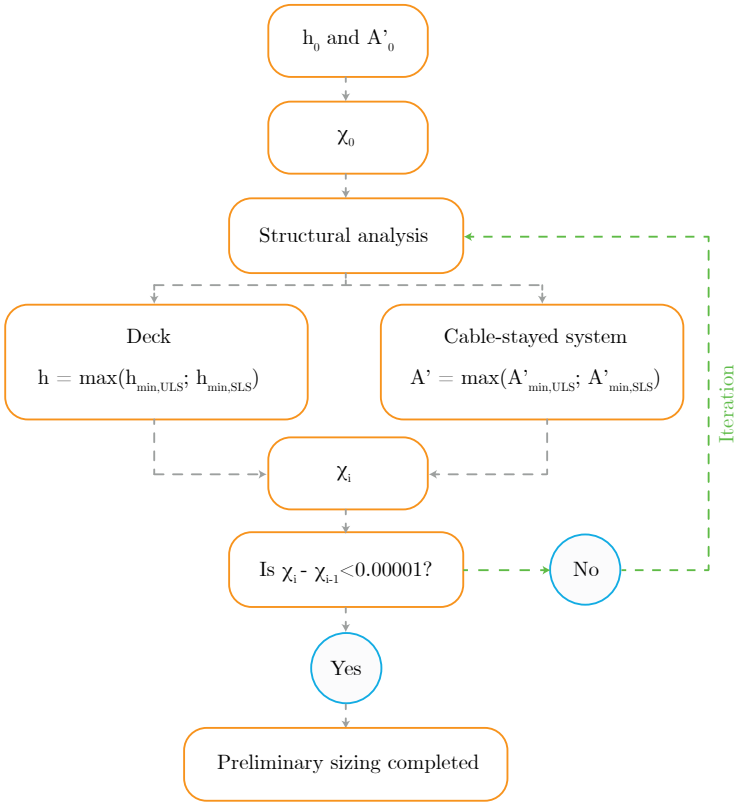

Figure 4.3: Workflow of the design process using the analytical formulation.

To obtain the variables in a simple way, the next methodology is used: first, initial values of h and A', randomly selected and defined as h_0 and A'_0, are given. With these values, χ is calculated and it is considered fixed until new values of h and A' are obtained. In the second step, each limit state is solved independently. The maximum A' which fulfills both conditions, one of them strictly, is taken. The same procedure is followed for the deck and allows to obtain a value of h. With these two new values of h and A', a new χ is calculated. This process is repeated until the error (difference of χ between two consequent iterations) is sufficiently small (specifically, less than 0.00001). This procedure results in values of h and A' which strictly fulfill two limit states (as marked in Figure 4.2). The methodology herein described has been implemented using Python language.

To understand the influence of the smart system on the design, different structures have been calculated, each with a different value of the degree of responsiveness (q_t/q_d). Specifically, 21 values of q_t/q_d are considered, ranging from fully smart structures ($q_t/q_d = 0.0$) to conventional structures ($q_t/q_d = 1.0$), with a difference of 0.05 among them. The results are presented in the next section.

4.3 Preliminary results

In all the following plots q_t/q_d is represented in the x-axis. This enables to show how the system behaves as q_t/q_d gradually increases, providing a notion of the influence of the smart system. The results for $q_t/q_d = 1.0$ allow comparison with a conventional cable-stayed system.

Figures 4.4a and 4.4b plot, respectively, the slenderness (L/h) versus q_t/q_d and the nominal cross-sectional area of the cable-stayed system (A') versus q_t/q_d, and the governing limit state in each case.

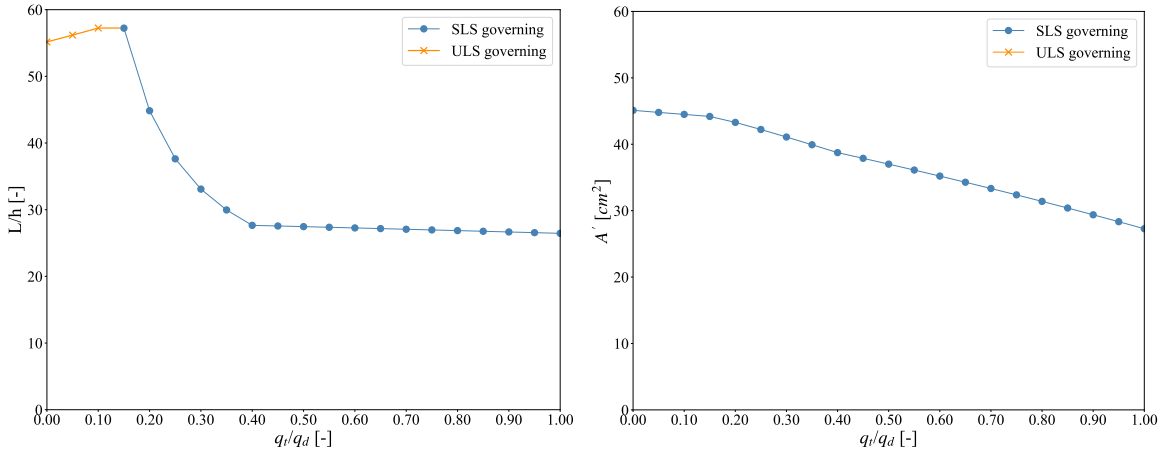

(a) Slenderness (L/h) of the deck vs. q_t/q_d.

(b) Nominal area (A') of the cable-stated system vs. q_t/q_d.

Figure 4.4: Dimensions of the smart under-deck cable-stayed footbridge, for varying values of q_t/q_d.

In Figure 4.4a, three different tendencies can be observed. First, from $q_t/q_d = 0.00$ to $q_t/q_d = 0.15$, ULS governs the design (orange dot marker), whereas in the rest, SLS is the most restrictive limit state (blue x-marker). The maximum slenderness ($L/h = 57$), obtained for $q_t/q_d = 0.15$, is coincident with the change of the governing limit state. From this maximum to $q_t/q_d = 0.40$ there is an abrupt decrease of the slenderness. This tendency disappears when the live load threshold (q_t) is higher than the frequent live load (i.e., $q_t/q_d \geq 0.40$), as the maximum deflection is checked when the structure is still working as a conventional one, thus all structures within this zone are designed for the same load case scenario.

Overall, the comparison of the maximum value of L/h (57) with the conventional structure ($L/h \simeq 27$) proves the great saving of material that can be achieved in the deck using a smart system.

Figure 4.4b plots the cross-sectional area of the stay (A') versus q_t/q_d. SLS is always the governing limit state. When $q_t/q_d = 0.0$, the strut behaves as a fixed support, transferring all the live load to the stays, so the maximum area is required. As q_t/q_d increases, the contribution of the cable in bearing the live load is lower and, therefore, a smaller area is necessary. The trend line shows a quasi-linear decrease with a slight change of slope in $q_t/q_d = 0.15$ and in $q_t/q_d = 0.40$, coincident with the change of the tendency described in the previous plot. This proves that the design of the beam and the stays are strictly correlated.

To provide a better understanding of Figure 4.4a, next, Figure 4.5 shows the minimum h necessary to fulfill each limit state independently. In addition, the envelope is marked.

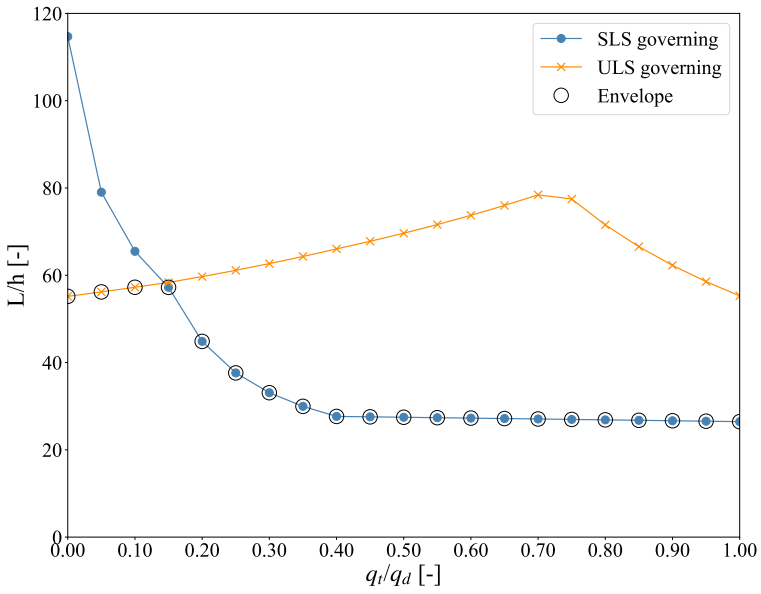

Figure 4.5: Slenderness (L/h) for each limit state individually vs. q_t/q_d.

The line plot obtained for SLS can be clarified as follows. As q_t/q_d increases, the deflections in the beam increase, requiring a higher value for h. As the maximum deflection is calculated for the frequent live load, the same slenderness is obtained for values of q_t/q_d between 0.4 and 1.0.

Regarding the results for L/h when only ULS is considered, when $q_t/q_d = 0.0$, the beam behaves as a two-span continuous beam under all load conditions. In this scenario, the design of the deck is conditioned by the midspan section, which experiences the highest negative bending moment. As the value of q_t/q_d increases, the proportion of the load q resisted by the smart system decreases. Consequently, a redistribution of bending moments occurs along the beam: positive bending moments increase while negative bending moments decrease. This

trend persists until a peak is reached, where the maximum positive bending moment equals the absolute value of the maximum negative bending moment (for $q_t/q_d = 0.70$). At this point, the slenderness attains its maximum value ($L/h \simeq 80$). For values of q_t/q_d greater than 0.70, the maximum positive bending moment progressively increases while the maximum negative bending moment decreases.

Figure 4.6a compares the stress in the cable-stayed system for the permanent state (σ'_g), and at SLS (σ'_{SLS}). The stress at SLS is constant ($0.45 \cdot f_{uk} = 706.5$ MPa) because the stays are designed to strictly fulfill this limit value at SLS. For the permanent state, the axial force ($F_{SLS]}$) in the cable-stayed system is identical in all cases, as the permanent load has been assumed constant. Consequently, for a lower cross-sectional area of the stay (A'), the stress under permanent loads (σ'_g) is higher.

For a specific value of q_t/q_d, the difference between σ'_{SLS} and σ'_g is the stress variation in the cable due to the live load. As q_t/q_d grows, the contribution of the stays in bearing the live load decreases, as well as the difference between both curves. Due to the singularity of this system, the limitation of F_{SLS} established by the code (Section 3.3.2) does not automatically guarantee a reduced live load stress increment, hence a specific fatigue verification has to be performed (Section 5.4.2).

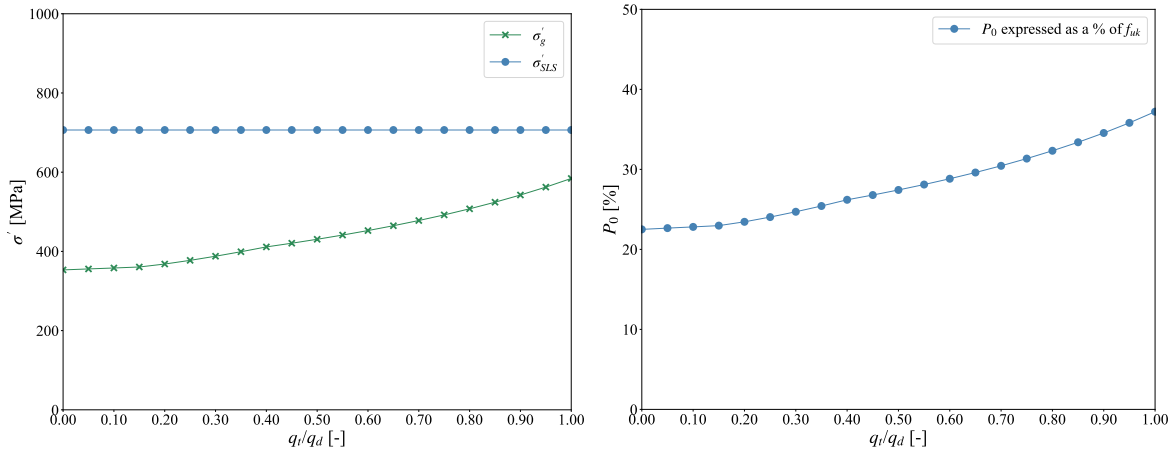

(a) Stresses (σ') vs. q_t/q_d.

(b) Initial prestressing (P_0) vs. q_t/q_d

Figure 4.6: Results at the cable-stayed system for varying values of q_t/q_d.

In Figure 4.6b the initial prestressing (P_0), expressed as a percentage of the ultimate tensile strength ($\%f_{uk}$), is plotted. It is observed that the value of the initial prestressing for the conventional structure, approximately 40% of f_{uk}, is very similar to the values described in Section 2.2. This proves that the results obtained are consistent. Regarding the fully

smart system, an initial prestressing of 22.5% of f_{uk} is obtained. This gives a preliminary idea of the design criteria that would define smart structures.

In summary, incorporating a smart system allows for the design of more slender decks. Moreover, the specific limit state that governs the design depends on the value of q_t/q_d. In contrast, the cable-stayed system requires a higher cross-sectional area as the actuator compensates a higher portion of the live load. In order to evaluate at a bigger scale which system is more convenient, a cost and environmental analysis is conducted in Chapter 6.

Based on these results, the next section presents a parametric analysis addressed to investigate the role of the main parameters in the design.

4.4 Parametric analysis

4.4.1 Live-to-dead load ratio

The aim of this first parametric analysis is to determine how the effectiveness of a smart system varies for different values of the live-to-dead load ratio (q/g). Six different configurations, in which q/g gradually decreases from $q/g = 3.0$ (lightest solution) to $q/g = 0.5$ (heaviest solution), are designed. In all cases, the live load is kept constant to a value of $q = 5$ kN/m^2, which corresponds to the design live load for footbridges [78]. The results shown in the previous Section 4.3 were obtained for $q/g = 1.0$.

As q is constant and g varies, the sum $(g + q)$ also varies. Therefore, the results for different values of q/g can be compared only in a relative manner. In this parametric analysis, the design of the cable-stayed system (A') does not yield noteworthy results. Regardless of whether the design is governed by SLS or ULS, as g increases, A' grows linearly.

Figure 4.7 summarizes the slenderness of the deck (L/h) versus q_t/q_d for different values of q/g. In each graph, two line plots are represented, each obtained for only fulfilling one limit state (same procedure as in Figure 4.5). The envelope is obtained as the most restrictive of the two limit states.

When SLS is governing, the design only depends on q and, since it is constant in all cases, the SLS curves are almost identical. Slight differences are due to small changes in the cross-sectional area of the cables (A'). When ULS governs the design of the deck, as it depends on $g + q$, it is more restrictive as q/g decreases.

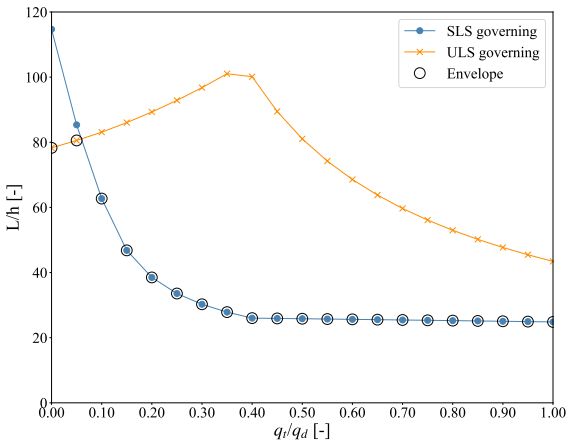

(a) L/h vs. q_t/q_d for $q/g = 3.0$.

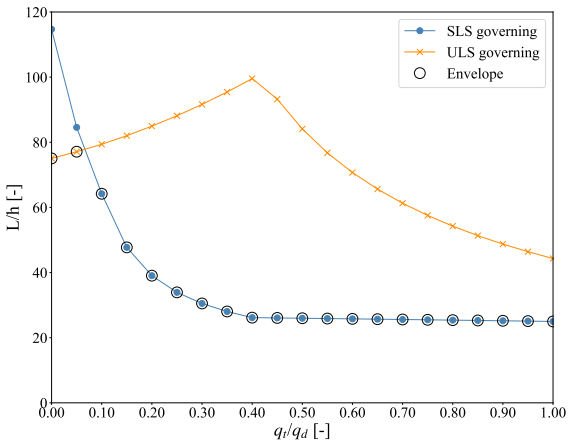

(b) L/h vs. q_t/q_d for $q/g = 2.5$.

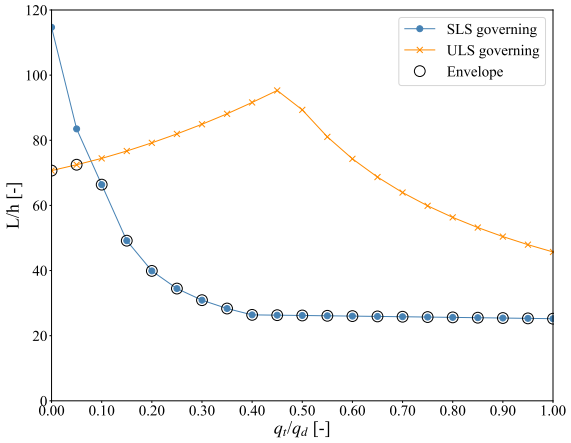

(c) L/h vs. q_t/q_d for $q/g = 2.0$.

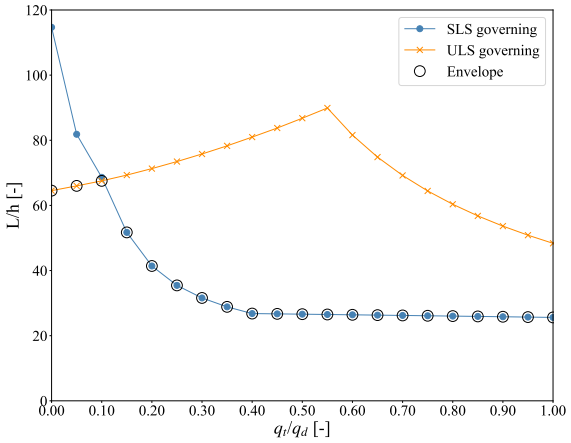

(d) L/h vs. q_t/q_d for $q/g = 1.5$.

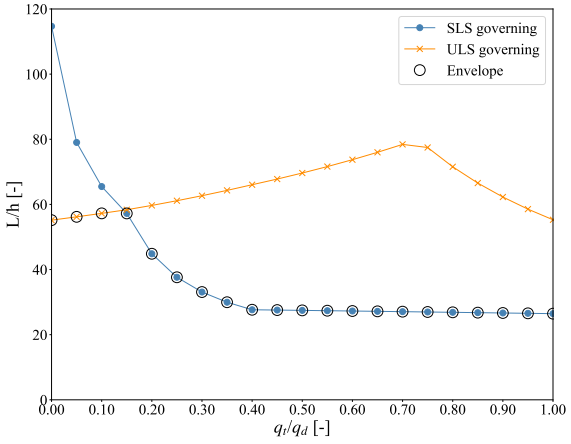

(e) L/h vs. q_t/q_d for $q/g = 1.0$.

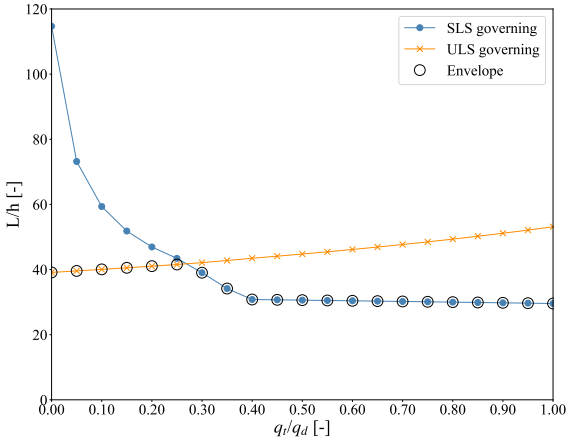

(f) L/h vs. q_t/q_d for $q/g = 0.5$.

Figure 4.7: Slenderness (L/h) versus q_t/q_d for different values of q/g.

Therefore, as the q/g ratio reduces, the value of q_t/q_d at which the maximum slenderness is obtained increases. While in $q/g = 3.0$ the maximum slenderness ($L/h \simeq 81$) is obtained for $q_t/q_d = 0.05$, for $q/g = 0.5$ the peak ($L/h \simeq 42$) corresponds to $q_t/q_d = 0.30$. The lighter the structure, the less restrictive ULS will be, leading to a more slender structure.

As a main conclusion, smart structures are most effective when live loads are significantly high in comparison to permanent loads. Therefore, if light materials, such as steel or fiber-reinforced polymer, are used for the deck, the benefits of the smart system can be maximized.

4.4.2 Rise-to-span ratio

The second parametric analysis aims to establish the influence of the rise (f) when designing smart under-deck cable-stayed structures. The span is kept constant ($L = 50$ m) and the strut length varies, covering a range from $f = 0.01$ m ($f/L = 0$) to $f = 50$ m ($f/L = 1$). These limits are not realistic, but provide a better insight of the repercussions of varying the rise-to-span ratio (f/L).

The results obtained from this parametric analysis are plotted in Figure 4.8. In both graphs, f/L is represented in the x-axis. Six different lines, for different values of q_t/q_d, are plotted.

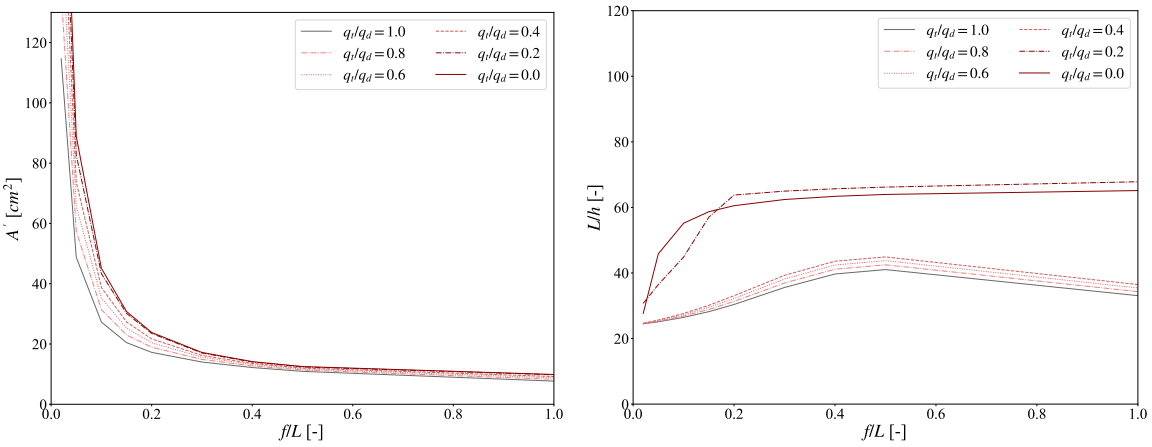

(a) A' vs. f/L. **(b)** Slenderness (L/h) vs. f/L.

Figure 4.8: Parametric analysis: rise-to-span ratio (f/L).

In Figure 4.8a, f/L is plotted versus the cross-sectional area of the cable-stayed system (A'). By increasing f/L, the angle (α) formed between the stays and the deck increases.

Consequently, for an unvaried vertical force transmitted by the strut to the cable, as α increases, the horizontal component of the axial force in the cable decreases, resulting in a smaller area of the stay. This behavior is independent on q_t/q_d. For a fixed f/L, as q_t/q_d increases, the area of the cable-stayed system grows, which is consistent with the results obtained before.

Figure 4.8a shows that it is worth avoiding small values of the rise, as they would require very high values of A' (left side of the plot). A relevant saving of material can already be achieved by using a rise-to-span ratio of 0.10. There are no evident benefits in employing rise-to-span ratios higher than 0.20, as the savings achieved by reducing the area would be very small compared to the associated cost of increasing the strut and stay length.

Figure 4.8b plots the slenderness of the deck versus the span-to-rise ratio. For a specific value of f/L, the same results as before are obtained: L/h increases with q_t/q_d, but there are no changes when the live load threshold is higher than the frequent live load ($q_t/q_d > 0.4$). The higher values of L/h are obtained for $q_t/q_d = 0.20$, from where there is a big gap with $q_t/q_d = 0.40$, a result which is consistent with the rapid decrease of slenderness plotted in Figure 4.4a. Essentially, this tendency maintains as f/L varies. For a fixed value of q_t/q_d, L/h grows rapidly as f/L increases until $f/L \simeq 0.2$, from which the increase of slenderness is almost negligible. This is because as f/L increases (α increases), so does ξ. Hence, even if the area of the cable-stayed system reduces, as the ξ increases, bending moments in the beam are reduced, allowing to design more slender decks. This tendency is very subtle when $q_t/q_d > 0.4$.

In conclusion, the optimal rise-to span ratio, both for the stays and the deck, is found between 0.10 and 0.20. Whereas in the stays this behavior is independent of q_t/q_d, the benefits achieved in the deck for the indicated f/L range are emphasized for low values of q_t/q_d.

4.4.3 Optimum span range

The present section aims to determine the optimal span range for partially smart under-deck cable-stayed structures. Different values of the span, from $L = 15$ m to $L = 200$ m, are studied, being $L = 50$ m the reference span used in the other analyses.

The parameters used to evaluate the optimum span are the increase of slenderness (L/h) and the reduction of weight per square meter (kg/m^2), compared to a conventional structure ($q_t/q_d = 1.0$). Both ratios only express variations in the deck, as A' varies linearly with the

span.

The first ratio is expressed as a percentage of the maximum increment in slenderness ($\Delta(L/h)$) compared to that of a conventional structure:

$$\Delta(L/h) = \frac{(L/h)_{max} - (L/h)_{q_t/q_d=1.0}}{(L/h)_{q_t/q_d=1.0}} \quad [\%] \tag{4.20}$$

The second ratio represents the maximum reduction in weight per unit surface area ($\Delta(W/m^2)$) compared to that of a conventional system.

$$\Delta(W/m^2) = \frac{(W/m^2)_{q_t/q_d=1.0} - (W/m^2)_{min}}{(W/m^2)_{q_t/q_d=1.0}} \quad [\%] \tag{4.21}$$

It is important to note that the values of q_t/q_d that yield the maximum slenderness and the minimum weight differ in each scenario.

In the following graphs, these ratios (y-axis) are plotted versus the span (L) (x-axis). Three different lines are depicted, each one representing a different value of the permanent load: $g = 2.5$ kN/m^2, $g = 5$ kN/m^2 and $g = 10$ kN/m^2. This will enable the evaluation of the optimal span range for varying values of q/g and, consequently, for different types of bridges.

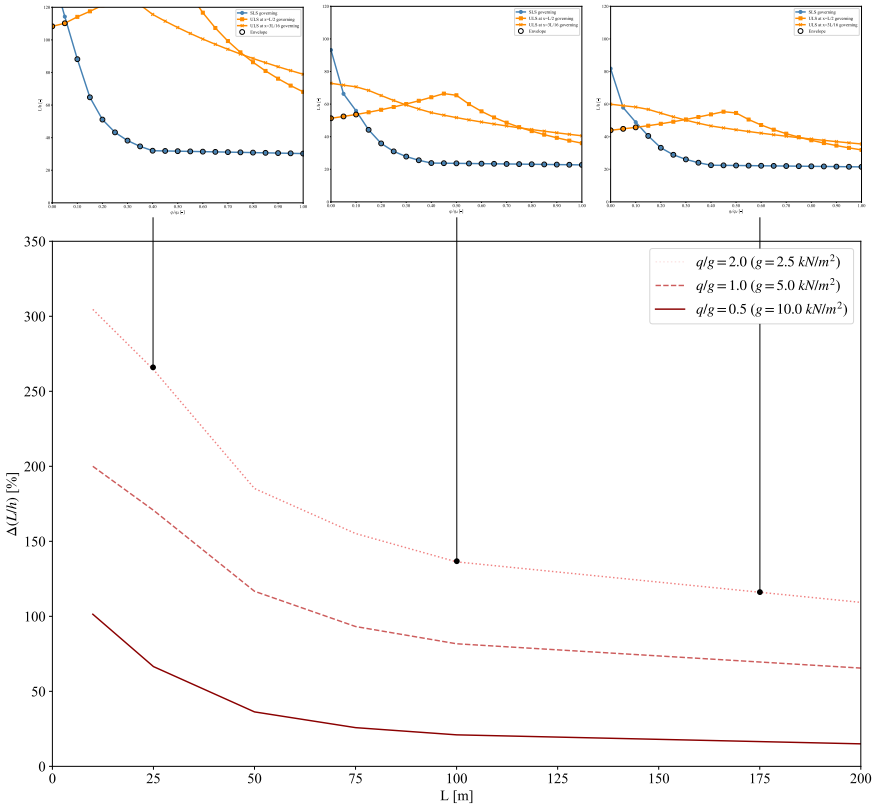

Figure 4.9: Optimum span range. $\Delta(L/h)$ versus span (L).

Figure 4.9 illustrates how, as expected, the increase in span results in a decrease in slenderness. This trend is more pronounced for lighter structures, so by observing the variation in $\Delta(L/h)$, it can be concluded that the advantages of a smart structure are most pronounced for lighter structures with shorter spans. Additionally, three graphs depicting the slenderness versus q_t/q_d are presented to demonstrate that the maximum L/h is achieved for a different value of q_t/q_d in each case.

In contrast, if we examine the weight of the deck per unit surface area (Figure 4.10), this behavior is reversed. As the span increases, the reduction in weight achieved in the deck becomes more significant. Once again, this pattern is more accentuated for lighter structures.

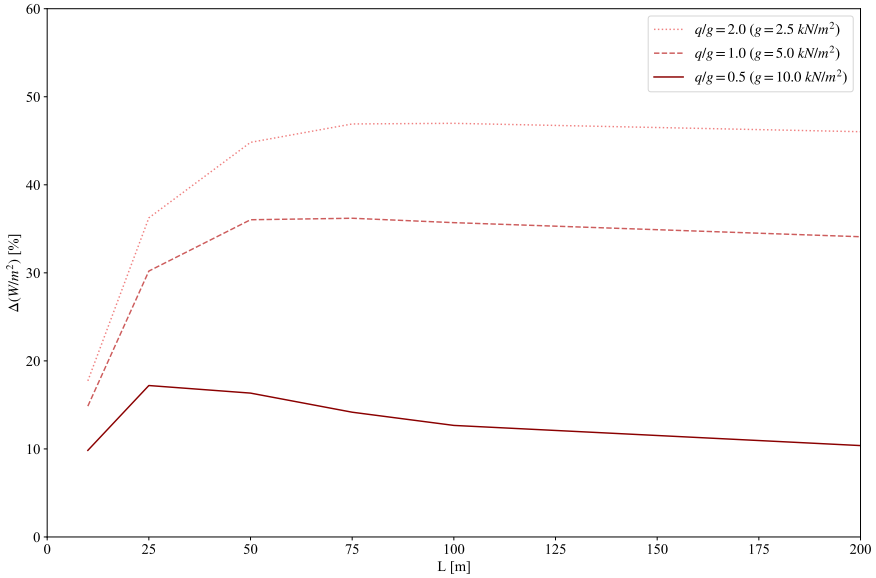

Figure 4.10: Optimum span range. $\Delta(W/m^2)$ vs. span (L)

Based on the findings of this parametric analysis, two key conclusions can be drawn. Firstly, smart under-deck cable-stayed structures demonstrate their optimum performance for spans ranging from short to medium lengths, between $L = 25m$ and $L = 75m$. Beyond this span range, notable benefits are not observed. Secondly, the influence of the total span on both slenderness and weight per surface area is more significant for lighter structures.

4.4.4 Influence of the mechanical properties

Finally, this section briefly discusses how the mechanical properties impact the design of partially smart systems. Each case assumes that all other parameters remain invariant.

- **Young modulus of the deck ($\mathbf{E_s}$) and the cable-stayed system ($\mathbf{E'_s}$).**
  The influence of Young's modulus on the structural behavior of the system is assessed by examining their relationship: $n = E'_s/E_s$. As the value of n increases, the efficiency of the system (ξ) also increases, necessitating a larger area (A').
  The impact of n on the design of the deck depends on the governing limit state. If ULS governs the design, an increase in the parameter ξ enables a reduction in the height (h). However, if SLS governs the design, as n increases, the Young's modulus of the deck decreases. Consequently, in order to maintain the maximum allowable deflection at the beam ($L/1200$), a higher inertia is required. Thus, even with an increased area of the cable-stayed system, the height of the deck cannot be decreased. This underscores the significance of maintaining an appropriate balance between both E_s values; otherwise, the advantages of utilizing a cable-stayed system would be misused.
- **Yield strength ($\mathbf{f_{sy}}$) of the steel of the deck.**
  The design of the beam is affected by changes in the yield strength (f_{sy}) only when ULS governs. An increase in f_{sy} results in a reduced required height (h).
  For example, if observing Figure 4.5, this would cause the ULS plot lines to shift upward (i.e., higher L/h for the same q_t/q_d). As a result, the intersection point with the SLS plot line (optimum design) occurs at a higher value of L/h and a lower value of q_t/q_d.
- **Ultimate tensile strength ($\mathbf{f_{uk}}$) of the cable-stayed**
  The value of f_{uk} influences the required area of the cable-stayed system. When f_{uk} increases, a smaller area is needed to withstand the same tension force, and conversely, when f_{uk} decreases, a larger area is required.

This brief discussion highlights the influence of varying the mechanical properties on the optimal degree of responsiveness, as well as the correlation of the deck and the cable-stayed system, wherein changes in one parameter impact the design of both elements.

Next, in Chapter 5, the same analysis is performed employing a numerical methodology.

5

Numerical FE simulation

5.1 Introduction

The analytical formulation (Chapter 4) allowed to obtain an overview on the design of smart under-deck cable-stayed structures. Nonetheless, it is based on a series of simplifications, as described in Section 4.1. Therefore, to overcome these limitations and obtain more accurate results, a Finite Element Model (FEM) is developed.

The under-deck cable-stayed system is modeled in SOFiSTiK (Figure 5.1), a FE software for structural analysis. Cross-sections and materials have already been described in Section 3.3.1. In order to obtain accurate results, 100 beam elements (and thus 101 nodes) are used to model the deck. For the stays, cable elements (only tension forces allowed) are employed, modeled in order to replicate the behavior of fully locked cables. The actuator is modeled as an infinitely stiff beam element in which the elongation is simulated by introducing a strain in the axial direction. A linear analysis is performed. The formulation for beam elements used in SOFiSTiK considers shear deformation and hinge effects.

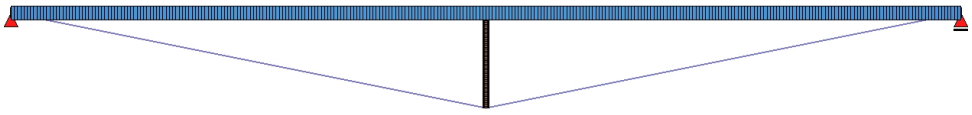

Figure 5.1: 2-Dimensional numerical model of the smart under-deck cable-stayed footbridge.

The numerical approach eliminates the simplifications assumed in the analytical formulation, providing a more accurate prediction of the structural behavior. The control sections are not limited to $x = 3L/16$ and $x = L/2$ and the design value of the maximum stress in the deck (σ_{Ed}) is obtained as the maximum Von Mises stress along the whole deck.

Additionally, three different alternatives are considered regarding the position of the live load. The introduction of these new load patterns causes a more restrictive design of the deck. Despite that, although the numerical approach provides more accurate results, the analytical results are still valid for a preliminary analysis.

In addition to the ULS and SLS verifications, the ALS (in which the actuator stops working) is verified, as well as some additional verifications detailed in Section 5.4.

5.2 Design workflow

The design procedure is represented in Figure 5.2. An iterative process, using the parametric input language CADINP, is implemented in SOFiSTiK to obtain, for each value of q_t/q_d, the minimum dimensions of the deck and cable-stayed system. Specifically, the height of the beam (h) and the diameter of the cable-stayed system (D') are the target variables to be minimized. The structure is designed to fulfill all applicable limit states in the beam and the stays (see Section 3.3.2). As a simplification, only one cable is considered. However, as indicated in Section 3.3.2, it is recommended to use multiple cables to guarantee sufficient structural redundancy.

To simplify the calculations and to provide realistic dimensions, the value of h is forced to a be multiple of 5 cm and the diameter of the cables (D') to a multiple of 5 mm. Only fully locked cables with commercial dimensions are considered. A consequence of restricting the values of h and D' is that, in most cases, it is not be possible to strictly fulfill the limit states. Thus, the criterion to define those dimensions is that the material utilization of both the deck and the cable-stayed system must be between 0.9 and 1.0.

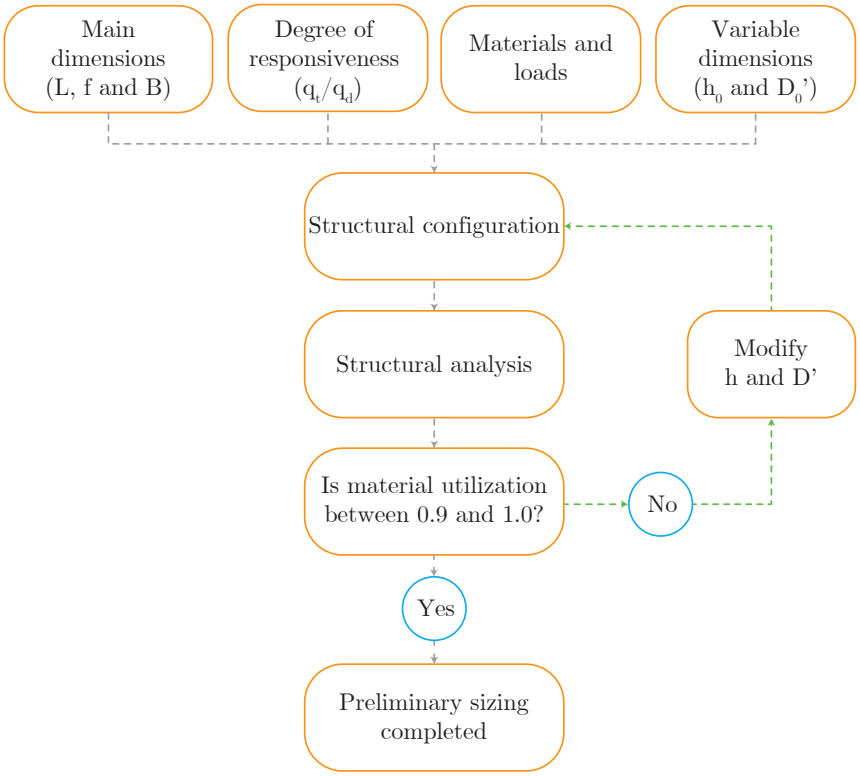

Figure 5.2: Workflow of the design process used in the numerical simulation.

As highlighted in Chapter 4, the results obtained for values of q_t/q_d higher than 0.4 are not noteworthy, due to the limitation imposed by SLS at the deck, resulting in identical outcomes. Consequently, only two values within the range of $q_t/q_d = 0.4$ to $q_t/q_d = 1.0$ are chosen for analysis, specifically 0.50 and 0.75, as they provide sufficient insight into the system's performance.

5.3 Results

This section presents the results obtained through the numerical formulation. Similarly to Section 4.3, the following plots depict the influence of the smart system by representing q_t/q_d on the x-axis. Additionally, the results for $q_t/q_d = 1.0$ are included to enable a comparison with a conventional cable-stayed system (i.e., without smart behavior).

In Figure 5.3, the results obtained for the dimensions of the beam (slenderness) are plotted versus q_t/q_d. A maximum slenderness equal to $L/h = 53$ ($h = 0.95$ m) is accomplished

for $q_t/q_d = 0.20$ and $q_t/q_d = 0.15$. Although the maximum slenderness is lower than the analytically calculated ($L/h = 57$), it is reached for the same value of q_t/q_d, providing consistent results. The three tendencies described in Section 4.3 can also be identified in this plot.

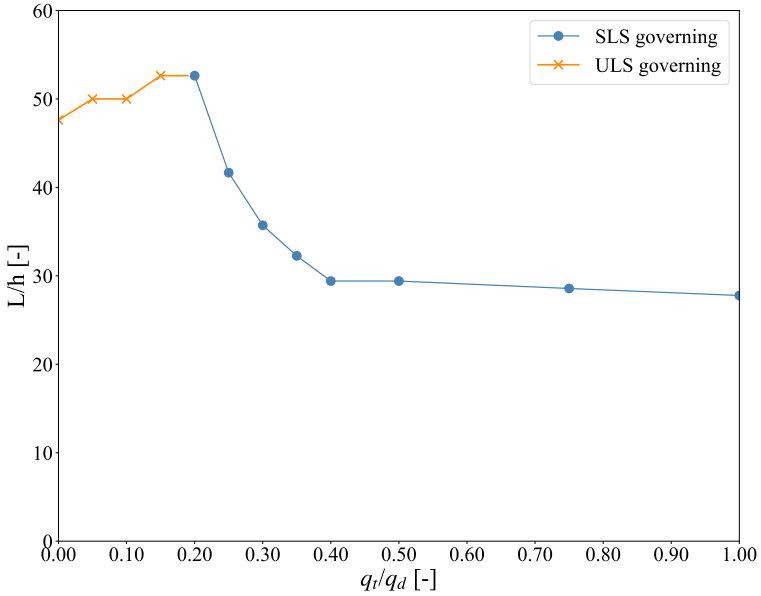

Figure 5.3: Slenderness (L/h) of the beam vs. q_t/q_d.

The results of the cross-sectional area of the cable-stayed system (A') are not displayed as A' is constant for most values of q_t/q_d, due to the limited number of options available within the necessary range.

In Figure 5.4a, the vertical displacements due to the frequent live load are plotted versus q_t/q_d. The dash line represents the maximum displacement ($L/1200$). The two solid lines represent the vertical displacement at midspan and the maximum vertical displacement along the beam. The maximum vertical displacement is generally found at midspan when q_t/q_d is high, as deflections are checked before the actuator has begun to move. Figure 5.4a also reveals when SLS is the governing limit state. When $q_t/q_d > 0.35$, u_z is very close to the dashed line, indicating that SLS governs the design of the deck.

Figure 5.4b shows the maximum Von Mises stresses in the beam at ULS. As expected, these stresses are close to the limit ($f_{sy} = 235$MPa) when ULS is governing the design; this demonstrates the high material utilization achieved in the beam when the degree of responsiveness is high.

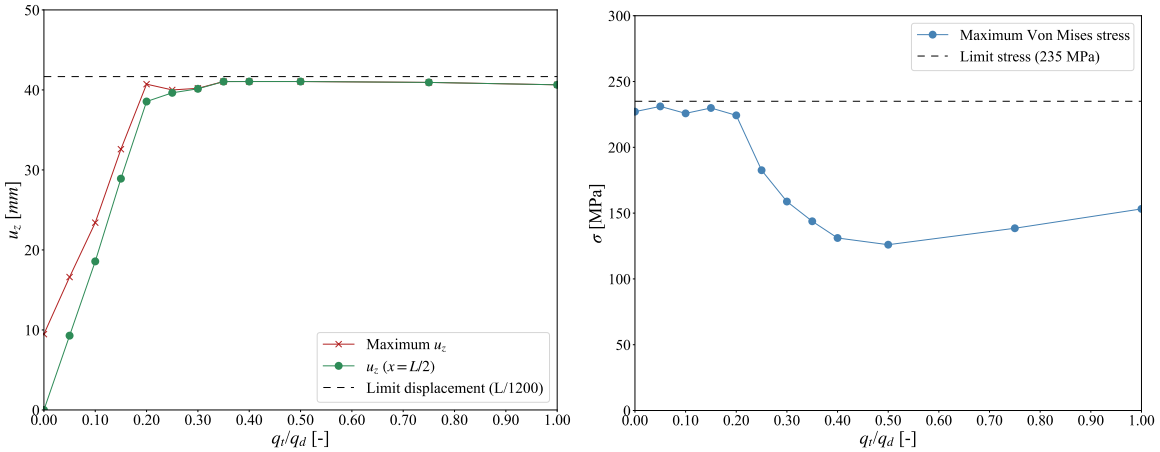

(a) Displacements caused by frequent live load at the deck vs. q_t/q_d.

(b) Von Mises stress (σ) in ULS at the deck vs. q_t/q_d.

Figure 5.4: Results at the deck obtained from the numerical procedure for varying values of q_t/q_d.

For $q_t/q_d = 0.20$, the material utilization is also very high, even if SLS governs the design (i.e., the maximum vertical displacement is close to $L/1200$). This proves that, for this specific value of q_t/q_d, the smart system allows to optimize the design of the beam, as both limit states are almost strictly fulfilled.

Finally, the results for the cable-stayed system are shown in Figure 5.5. These results are similar those shown in Figure 4.6 (obtained with the analytical formulation), although here the tendency is not as clear as before, due to the limitations imposed by the fixed values of D' and h.

Figure 5.5a plots the stress in the cable-stayed system plotted for the permanent state and at SLS. The stress at SLS (σ'_{SLS}) is the condition governing the design of the cables, set to $0.45 \cdot f_{uk} = 706.5$ MPa. The value plotted in Figure 5.5a depends on the material utilization achieved in each case. Figure 5.5b depicts the initial prestressing, expressed as a percentage of the ultimate tensile strength. The minimum P_0, which is around 24% of f_{pu}, is obtained for $q_t/q_d = 0.20$.

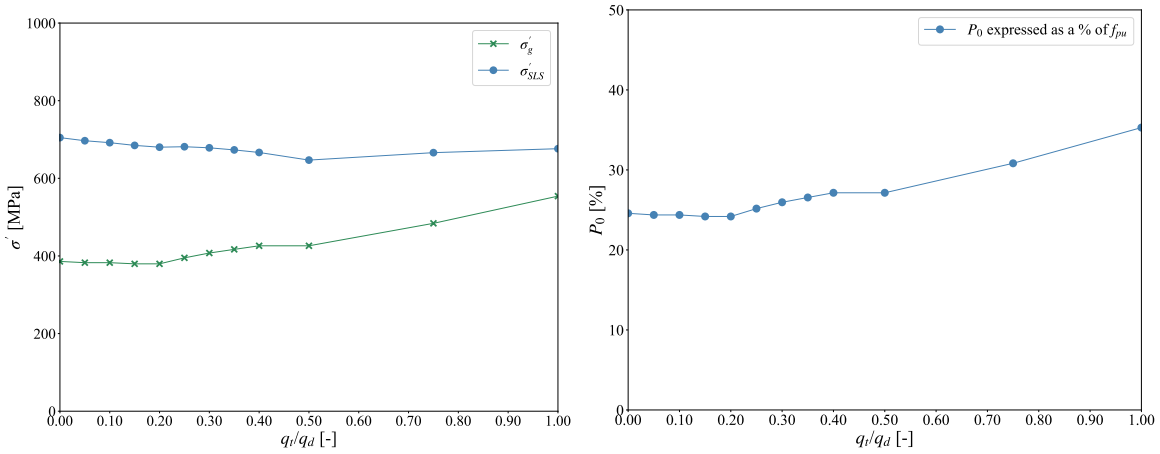

(a) Stresses (σ') vs. q_t/q_d.

(b) Initial prestressing (P_0) vs. q_t/q_d

Figure 5.5: Results at the cable-stayed system for varying values of q_t/q_d.

Additionally, it has been confirmed that the ALS of the actuator shutdown is verified for all the cases designed, never governing the design. The same finding has been obtained regarding buckling. Finally, in the next section some additional verifications, which were not initially incorporated into the design workflow, are conducted to assess vibrations in the deck and fatigue in the cables.

5.4 Other verifications

5.4.1 Dynamic analysis

Regardless of whether an analytical or a numerical approach is used, the smart under-deck cable-stayed footbridge is considerably lighter than a conventional structure. As a consequence, it can be susceptible to human-induced vibrations. Therefore, a dynamic analysis, based on the recommendations given in the HiVoSS Guidelines [79], is performed. This analysis is carried out on the structure designed with $q_t/q_d = 0.20$, as it presents the highest slenderness. The procedure follows the methodology described in [79]:

1. Evaluation of natural frequencies. They are obtained from a modal analysis of the FEM of the system. The masses considered in the analysis are the self-weight of the deck and the superimposed dead load. The mass of the actuator is neglected. The analysis is performed considering a diagonal, also known as lumped, mass matrix.

2. Check of the critical range of natural frequencies. The critical ranges of the natural

frequencies of footbridges with pedestrian excitation are 1.25 to 4.60 Hz for vertical and longitudinal vibrations, and 0.50 to 1.20 Hz for lateral vibrations [79]. From the eigenvalues obtained from the FEM, only one natural frequency (f_i) is within the critical ranges: the second vertical vibration mode has a frequency of 2.587 Hz.

As the footbridge is susceptible to vibrate, a more detailed dynamic analysis is performed.

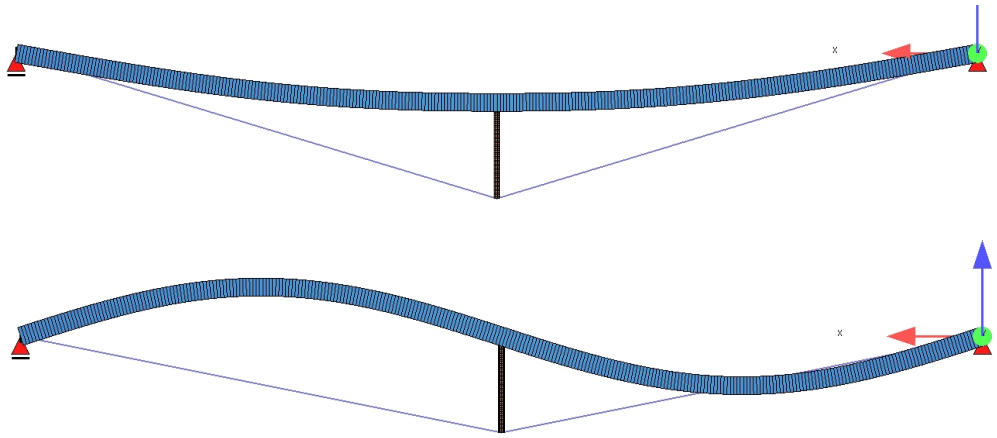

Figure 5.6: First ($f_1 = 1.160$ Hz) and second ($f_2 = 2.587$ Hz) vertical vibration modes.

3. Assessment of the design situation. The dynamic analysis is done considering a traffic class TC4, that is expected to occur once in the lifetime of the footbridge (e.g., inauguration of the footbridge). For this traffic class, table 4-3 of HiVoSS [79] establishes a pedestrian density of $d = 1$ P/m^2.

4. Evaluation of the maximum acceleration (a_{max}). To calculate the maximum acceleration, an harmonic load model is applied to the structure. A pedestrian stream of n random pedestrians is modeled as an idealized stream of n' perfectly synchronized pedestrians.

   The harmonic distributed load that represents this equivalent pedestrian stream is $p(t)[\text{N/m}^2] = P \cdot cos(2 \cdot \pi \cdot f_s \cdot t) \cdot n' \cdot \Psi$ [79]. Where f_s is the step frequency, assumed equal to the footbridge natural frequency under consideration ($f_s = 2.587$ Hz), $P = 280$ N is the component of the force due to a single pedestrian with a walking step frequency f_s and n' is the equivalent number of pedestrians on the loaded surface ($S = L \cdot B = 200\text{m}^2$; being $L = 50$ m the span of the footbridge and $B = 4$ m its width). For the considered Traffic Class, it is calculated as $n' = 1.85 \cdot \sqrt{n}/S = 0.1308$, being n the number of pedestrians of the loaded surface ($n = S \cdot d = 200\ P$).

   Finally, Ψ is a reduction coefficient that considers the probability that the footfall

frequency approaches the critical range of the natural frequency under consideration. For $f_s = 2.587$ Hz, the norm establishes a value of Ψ between 0 and 0.25. A conservative value of $\Psi = 0.25$ is considered.

Finally, a_{max} is obtained by applying the harmonic load $p(t)$ to the FE model. The distribution of $p(t)$ in the structure corresponds to the modal shape under consideration. A modal steady-state analysis is performed and a maximum acceleration of $a_{max} = 0.57$ m/s^2 is obtained.

5. Checking of comfort levels. The maximum acceleration, $a_{max} = 0.57$m/s^2, corresponds to a medium comfort level (CL2). Therefore, the vibration limit state is verified even for a rarely expected scenario.

5.4.2 Fatigue in the cable-stayed system

The elongation of the actuator causes an increase of tension in the stays. If this movement is repeated continuously, failure in the stays due to fatigue can occur.

As discussed in Section 2.2.2, the codes and manufacturers provide a maximum stress increment that can be tolerated by the cables. These values are applicable until $2 \cdot 10^6$ load cycles, so by fulfilling this restriction the fatigue limit state is automatically verified. However, higher stress ranges can be assumed if it is demonstrated that the number of cycles during the whole life of the structure will be lower. To perform the fatigue check, the cumulative damage method proposed by Part 1–9 of the EC3 [22] is used.

Again, the analysis has been carried out on the structure designed with $q_t/q_d = 0.20$. The study proceeds by following the next steps:

1. Obtain the stress history from the loading sequence. Then, calculate the stress variation ($\Delta\sigma$) in the stays caused by each value of the traffic live load.

2. Count the number of cycles of each stress range. The number of times each load occurs is calculated using the definition of probability of occurrence given by the Eurocodes [77]. The number of cycles is taken as the number of times each load is exceeded. A more detailed explanation of this procedure can be found in Chapter 6, as the same approach is followed to calculate the energy consumption of the actuator.

3. Determine the cycles to failure at each stress range. This is done using the Wöhler curve of the material. Figure 9.1 of Part 1–11 of the EC3 [22] provides the curve for fully locked cables, with $\Delta\sigma_c = 150$ MPa (maximum stress range for $2 \cdot 10^6$ cycles).

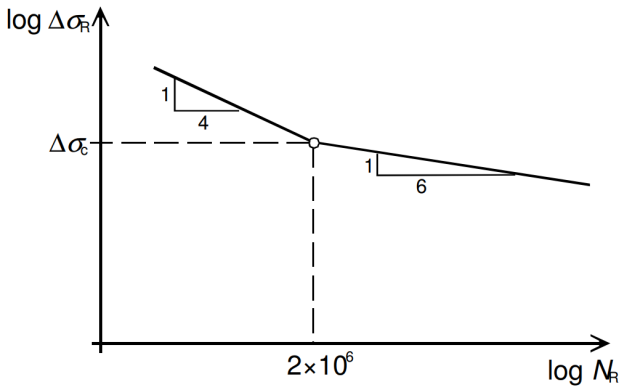

Figure 5.7: Figure 9.1 of Part 1–11 of the EC3 [22]: Fatigue strength curves for tension components.

4. Proceed to the damage summation using the Palmgren-Miner rule:

$$\sum \frac{n_i}{N_i} = D_d \tag{5.1}$$

Where n_i is the number of cycles at the stress range of each load, N_i is the number of cycles of failure for each load and D_d is the damage accumulation. If $D_d \leq 1$, the fatigue limit state is verified.

As the pedestrian live load reaches high values very rarely throughout the service life of the structure, a value of $D_d = 0.04$ is obtained, amply fulfilling the fatigue limit state in the stays.

6

Quantification of cost and environmental performances

6.1 Methodology

The findings presented in Chapters 4 and 5 highlight the potential for significant material savings in the deck by implementing a smart system. However, the necessary material for the cable-stayed system is increased, and the smart system introduces new elements that have to be taken into consideration. Therefore, a comprehensive analysis must be conducted to ascertain the actual benefits of employing a smart system. To address this objective, this chapter focuses on quantifying the performance of smart under-deck cable-stayed footbridges in terms of cost and CO_2 emissions. This is achieved through the implementation of a Life-Cycle Cost Analysis (LCCA) and a Life Cycle Analysis (LCA). The outcomes obtained from the numerical analysis conducted in Chapter 5 are used in this chapter.

While both methodologies aim to quantify the impact of processes and products throughout their life cycle, they differ in their focus. The LCCA primarily assesses the cost impact, whereas the LCA is focused on the environmental impact [81]. These analyses include the stages from the extraction of the material until the end of life, whether it is reused, recycled or disposed.

The environmental impact of a system is quantified by its carbon dioxide equivalent

emissions ($kgCO_2e$), taking into account the Whole Life Carbon (WLC). The WLC encompasses both the operational and embodied carbon emissions released throughout the entire lifespan of the asset. As the goal is to evaluate the benefits of using a smart system in comparison to a conventional one, only the stages that vary among the different cases are considered in the analysis. Figure 6.1 presents all stages of a Life Cycle Assessment (LCA), highlighting the modules evaluated in this study.

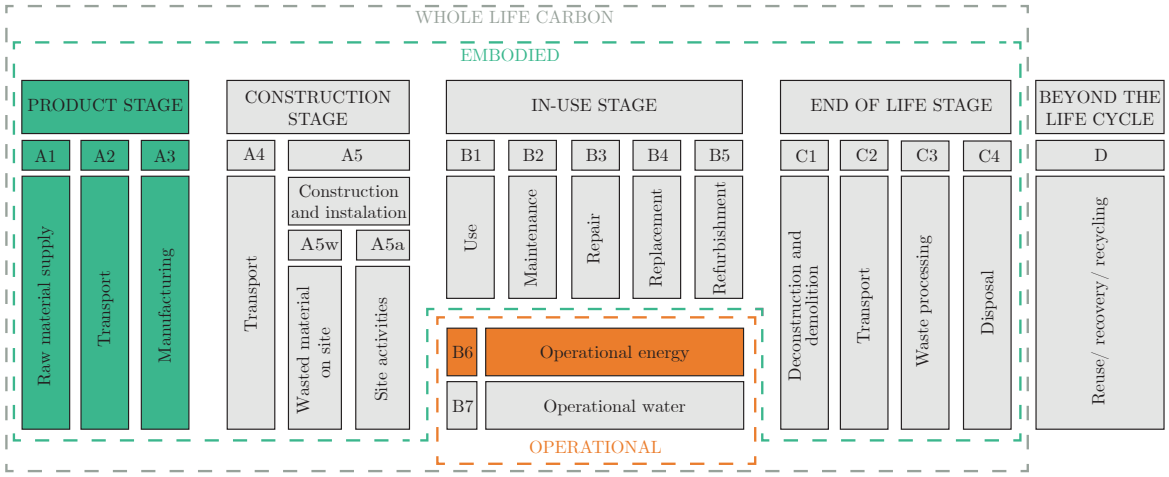

Figure 6.1: Scheme of the different stages considered in the Life Cycle Analysis (LCA). Adapted from [81].

The stages that exhibit variations when utilizing the smart system are the Product Stage (A1-A3) and the In-Use Stage (B). Specifically, in the In-Use Stage, only the operational energy (B6) is considered for simplicity. Although an exhaustive analysis would involve accounting for carbon consumption resulting from maintenance (B2), repair (B3), and replacement (B4) of the technological instrumentation, these factors have been disregarded in this study due to their minimal impact on the overall results. The same stages used for the LCA are used for the LCCA.

To summarize, the elements included in the analysis are the deck, made of steel (S235), the fully locked cables of the cable-stayed system, made of steel (Y1570C), and the electric actuator along with the energy consumption it requires for operation. Table 6.1 provides an overview of the unitary cost and carbon emissions associated with each unit.

Table 6.1 Unitary costs and emissions for the units of the smart under-deck cable-stayed footbridge.

Unit	Cost	ECC
S235 steel	1.94 €/kg	1.55 kg CO_2e/kg
Y1570C fully locked cables	14.86 €/kg	2.27 kg CO_2e/kg
Actuator	3200 €/unit	2000 kg CO_2e/unit
Operational energy	0.08 €/kWh	0.265 kg CO_2e/kWh

The embodied carbon emissions during the Product Stage (A1-A3) are determined by multiplying the quantity of each material by its Embodied Carbon Coefficient (ECC). For this analysis, the Institution of Civil Engineers DB 3.0 database is utilized, which is an openly accessible database created by the University of Bath [82]. The cost of each material is calculated by multiplying the respective quantity, as derived in Section 5.3, by its unitary cost. The material costs are sourced from a general construction Spanish database.

The cost of the electric actuator has been determined based on the information provided by personal communications with multiple actuator suppliers. This cost corresponds to the approximate market price for a maximum load capacity of 130 kN and a maximum stroke elongation of 30 cm. To simplify the cost estimation for each designed case, a linear relationship is assumed between the maximum load capacity of one actuator and the required load capacity for each value of q_t/q_d, assuming that several parallel actuators are employed when necessary.

The energy consumed by the electric linear actuator is obtained as follows:

$$\text{Electric energy [kWh]} = \frac{\text{Speed [m/s] x Force [kN] x Number of working hours [h]}}{\text{Efficiency [\%]}} \tag{6.1}$$

Typical values for the speed and efficiency of electric linear actuators are employed: 10 mm/s and 80%, respectively. The force and the number of working hours are obtained by making a series of assumptions. First, a working life of 50 years is considered, matching the footbridge's design life. The number of working hours of the actuator is derived using the probability of occurrence of each value of the live load. This probability is calculated using the definition of the representative load values given in Eurocode 0 [77] and their corresponding return periods:

- Characteristic value (1.0 q_d): once in a lifetime
- Infrequent value (0.7 q_d): once per year

- Frequent value (0.4 q_d): once per week
- Quasi-permanent (0.0 q_d): 50% of the reference period.

By taking into account the return period of the aforementioned loads and the average time required to cross the footbridge (estimated at two minutes), it is possible to calculate the number of hours that each load value, ranging from 0 to q_d, is reached over the system's operational lifespan. Consequently, based on the value of q_t, the corresponding number of operating hours of the actuator can be extrapolated.

As the force applied by the actuator depends on the acting live load, the calculation of energy consumption involves determining the average load over the system's operational lifespan. The force that must be operated by the actuator follows a lineal trend, from its corresponding value when the actuator starts working (when $q = q_t$) to its maximum value (when $q = q_d$). Considering this, together with the probability of exceeding each portion of q, as just calculated, the average force of the actuator is obtained. With these considerations, the electric energy consumed by the actuator, dependent on q_t/q_d, can be derived.

6.2 Cost and environmental analysis

In the subsequent analysis, the structures designed in Chapter 5 are evaluated using the methodology described above. As previously justified, partially smart structures for values of q_t/q_d higher than 0.4 do not yield significant results. Therefore, these values have been excluded from the results presented in this chapter. Only the $q_t/q_d = 1.0$ case is plotted to provide a direct comparison with the conventional system.

Figure 6.2 illustrates the relative costs (compared to the conventional structure) for different values of q_t/q_d. The plot demonstrates an increasing cost in the stays, actuator and energy as the smart system carries a greater portion of the live load. However, the cost of the beam exhibit an opposite behavior, with a minimum in $q_t/q_d = 0.15 - 0.20$. This minimum is coincident with the most cost-effective footbridge, achieving an overall cost saving of 13% for $q_t/q_d = 0.20$.

Figure 6.3 depicts the relative carbon footprint plotted against q_t/q_d, showing a similar trend as before. The results highlight that, again, the structure designed with $q_t/q_d = 0.20$ yields the lowest carbon emissions, achieving a substantial 23% reduction compared to the conventional system.

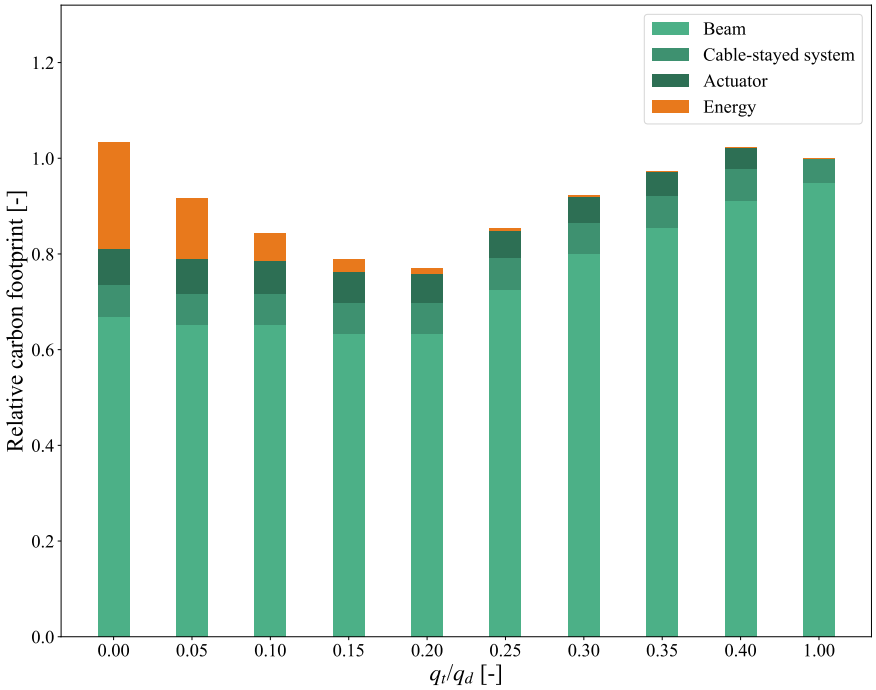

Figure 6.2: Relative cost of a 50-meter-span smart under-deck cable-stayed footbridge for different values of q_t/q_d.

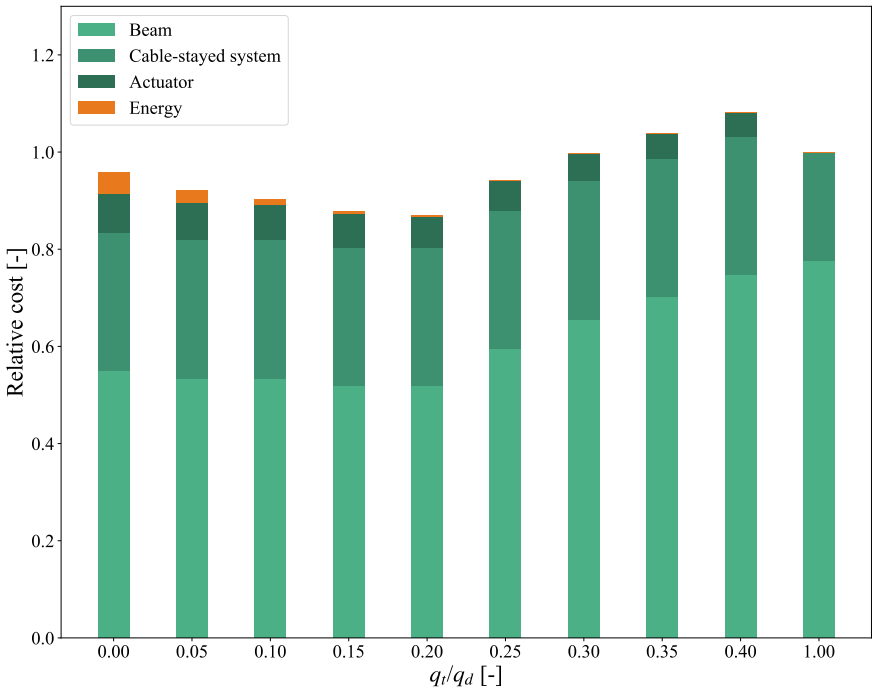

Figure 6.3: Relative carbon footprint of a 50-meter-span smart under-deck cable-stayed footbridge for different values of q_t/q_d.

6.3 Conclusions

The results demonstrate that a notable material reduction can be achieved by implementing partially smart systems in footbridges. Optimum outcomes are observed for values of q_t/q_d around 0.20, which corresponds to the scenario in which the actuator begins to work for any acting live load higher than 1 kN/m^2. This allows for an increase in the beam slenderness ratio from L/h = 27 (conventional structure) to L/h = 53 (partially smart structure), resulting in a material reduction of approximately 35% in the deck.

From an economic standpoint, a savings of 13% is achieved when comparing these two structures. In terms of carbon footprint, the partially smart structure exhibits a significant reduction of 23%, demonstrating the potential of smart structures to reduce environmental impact.

It is important to acknowledge that the values presented in Table 6.1 have been obtained from specific sources. To assess the applicability of these results to other contexts, a sensitivity analysis should be conducted. This analysis would evaluate the robustness of the findings by considering different sources for cost and carbon emissions data.

Furthermore, it is important to note that the optimization process outlined in Section 5.2 aimed to minimize the partial safety factors of both the deck and the cable-stayed system. To gain further insights, it would be valuable to investigate the cost and emission reductions that could be achieved if the design workflow was focused on minimizing each of these factors.